REVIEW

Mass spectrometry imaging with high resolution in mass and space

Andreas Römpp · Bernhard Spengler

Abstract Mass spectrometry (MS) imaging links molecular information and the spatial distribution of analytes within a sample. In contrast to most histochemical techniques, mass spectrometry imaging can differentiate molecular modifications and does not require labeling of targeted compounds. We have recently introduced the first mass spectrometry imaging method that provides highly specific molecular information (high resolution and accuracy in mass) at cellular dimensions (high resolution in space). This method is based on a matrix-assisted laser desorption/ionization (MALDI) imaging source working at atmospheric pressure which is coupled to an orbital trapping mass spectrometer. Here, we present a number of application examples and demonstrate the benefit of 'mass spectrometry imaging with high resolution in mass and space.' Phospholipids, peptides and drug compounds were imaged in a number of tissue samples at a spatial resolution of 5–10 μm. Proteins were analyzed after on-tissue tryptic digestion at 50-μm resolution. Additional applications include the analysis of single cells and of human lung carcinoma tissue as well as the first MALDI imaging measurement of tissue at 3 μm pixel size. MS image analysis for all these experiments showed excellent correlation with histological staining evaluation. The high mass resolution ($R = 30{,}000$) and mass accuracy (typically 1 ppm) proved to be essential for specific image generation and reliable identification of analytes in tissue samples. The ability to combine the required high-quality mass analysis with spatial resolution in the range of single cells is a unique feature of our method. With that, it has the potential to supplement classical histochemical protocols and to provide new insights about molecular processes on the cellular level.

Keywords Mass spectrometry imaging · Tissue analysis · High-resolution mass spectrometry · Accurate mass measurements · Mass spectrometry-based histology · MALDI mass spectrometry

Abbreviations

DHB	Dihydroxybenzoic acid
ESI	Electrospray ionization
H&E	Hematoxylin and eosin staining
LC	Liquid chromatography
MALDI	Matrix-assisted laser desorption/ionization
MS	Mass spectrometry
MS/MS	Tandem mass spectrometry
PC	Phosphatidylcholine
Ppm	Parts per million
RMS	Root mean square
SIMS	Secondary ion mass spectrometry
SM	Sphingomyelin
TOF	Time-of-flight (mass spectrometer)

A. Römpp (✉) · B. Spengler (✉)
Institute of Inorganic and Analytical Chemistry, Justus Liebig University, Schubertstrasse 60, 35392 Giessen, Germany
e-mail: andreas.roempp@anorg.chemie.uni-giessen.de

B. Spengler
e-mail: Bernhard.Spengler@anorg.Chemie.uni-giessen.de

Introduction: Mass spectrometry imaging

Mass spectrometry (MS) is a universal and prominent tool in analytical chemistry. This method can provide qualitative as well as quantitative information for a wide variety of compound classes. The molecular mass of a compound, calculated from the *m/z* value of the corresponding ion, can

be used for (tentative) identification. Ion fragmentation experiments (often called 'tandem MS' or 'MS/MS' experiments) provide information about the molecular structure of an analyte. Peak intensities in mass spectra can be calibrated for analyte quantitation. Mass spectrometry imaging combines these capabilities with information on the location of analytes within a sample. The spatial distribution can provide valuable additional information about the function and properties of an analyte, which would be lost in typical MS measurements of bulk (homogenized) samples. The first spatially resolved measurements in mass spectrometry were obtained with laser desorption ionization (LDI) in the 1970s (Hillenkamp et al. 1975a, b), but were limited to the analysis of smaller ions, predominantly of inorganic compounds. The investigation of larger (bio)molecules by mass spectrometry was made possible by the introduction of 'soft ionization methods,' namely electrospray (ESI) (Fenn et al. 1989) and matrix-assisted laser desorption/ionization (MALDI) (Karas et al. 1985; Karas and Hillenkamp 1988) in the 1980s. The first imaging application of MALDI was described in 1994 (Spengler et al. 1994). These experiments demonstrated that larger organic molecules such as peptides, which are thermally labile and which require matrix assistance, can be detected in a spatially resolved manner using a highly focused pulsed ultraviolet (UV) laser beam. This concept was taken up and extended to the analysis of tissue in the following years (Caprioli et al. 1997; Stoeckli et al. 2001). Today mass spectrometry imaging is one of the most active fields in mass spectrometry. While MALDI and secondary ion mass spectrometry (SIMS) (Boxer et al. 2009) are the most widely used ionization techniques for mass spectrometry imaging, a number of alternative techniques have been developed in recent years. In particular, atmospheric pressure ionization techniques such as desorption electrospray (DESI) (Eberlin et al. 2010), low-temperature plasma (LTP) (Liu et al. 2010) and laserspray ionization (Richards et al. 2011) are increasingly operated in imaging mode. MALDI can also be operated at atmospheric pressure (Laiko et al. 2000), but it has mostly been employed in high vacuum ion sources.

A schematic representation of a MALDI mass spectrometry imaging experiment is shown in Fig. 1. The sample (tissue section) is covered with matrix in order to allow desorption and ionization of bioorganic analytes. A laser beam illuminates a defined area of the sample and desorbs and ionizes material from the surface (Fig. 1a). The resulting ions are transferred to the mass spectrometer, and a mass spectrum is acquired (Fig. 1b). Subsequently, the sample is moved by a defined distance, and the next position on the sample is analyzed the same way. Several thousand spectra are typically acquired sequentially in this manner. MS images of a selected analyte peak are generated after the measurement by extracting the signal intensity within a certain m/z window. The intensities are plotted as gray scale values for each pixel in a grid representing the corresponding positions on the sample (Fig. 1c). These 'MS images' or 'selected ion images'[1] represent the spatial intensity distribution of a certain m/z signal, which can be assigned to a certain compound. Separate MS images can be generated for each signal in the mass spectrum. Therefore, mass spectrometry imaging is an 'untargeted' and multiplexed method. All desorbed and ionized compounds in the sample are detected, regardless of being known or unknown, expected or unexpected. This is a major advantage compared to other imaging techniques such as histochemical staining which requires the availability of a suitable antibody.

A number of compound classes have been analyzed by MALDI imaging including peptides (Chen et al. 2010; Stoeckli et al. 2002), proteins (Chaurand et al. 1999; Reyzer and Caprioli 2007), lipids (Jackson et al. 2005; Trim et al. 2008) and drug compounds (Stoeckli et al. 2007a). More details about MS imaging of these compound classes are covered in the respective sections below.

Today mass spectrometry imaging is used in a broad range of applications. The vast majority of studies are focusing on tissue originating from animal models or on human clinical tissue originating from surgical interventions. The targeted diseases include Parkinson's (Stauber et al. 2008) and Alzheimer's disease (Rohner et al. 2005) as well as Duchenne muscular dystrophy (Benabdellah et al. 2009b). Numerous studies of clinical tissue focused on cancer, for example prostate cancer (Cazares et al. 2009), breast cancer (Balluff et al. 2010), gastric cancer (Balluff et al. 2011a), adenocarcinoma (Djidja et al. 2009) and ovarian cancer (El Ayed et al. 2010). Additional topics in MS imaging studies included the analysis of plants (Lee et al. 2012; Kaspar et al. 2011; Peukert et al. 2011), insects (Vanickova et al. 2012) and microorganisms (Esquenazi et al. 2008; Yang et al. 2009).

A number of review articles about mass spectrometry imaging have been published in recent years. An extensive overview that covers instrumental topics as well as application areas is found in McDonnell and Heeren (2007). The main ionization techniques, namely MALDI, SIMS and DESI, are compared in Pól et al. (2010). The perspectives of MS imaging for clinical research focusing on protein analysis are covered in Rauser et al. (2010a) and Balluff et al. (2011b). A review by Schwamborn is specifically targeted at biomarker discovery approaches by MALDI

---

[1] The term 'MS image' will be used in this work to describe the outcome of an MS imaging experiment in a general meaning. 'Selected ion image' will be used when referring to the spatial intensity distribution of a specific ion.
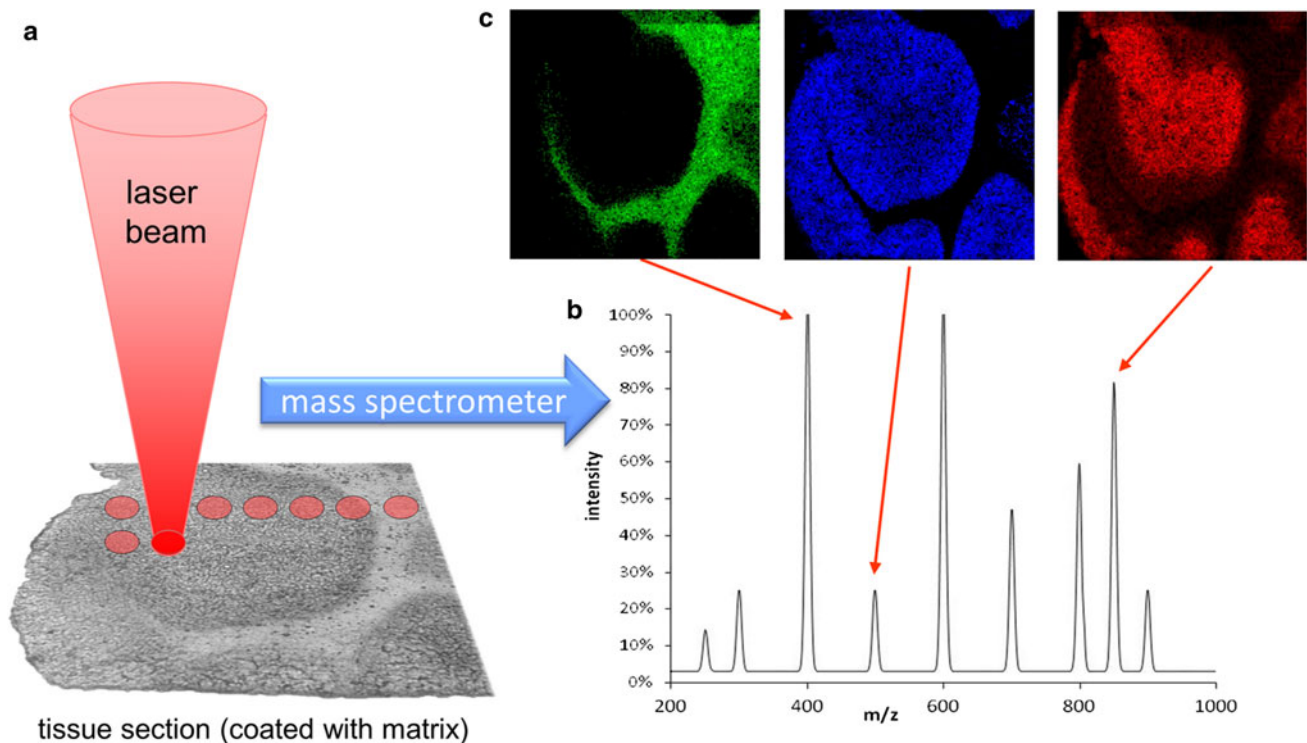
Fig. 1 Scheme of the mass spectrometry imaging process. **a** The tissue section is covered with matrix and irradiated by a pulsed laser beam. **b** Mass spectrum acquired from the tissue section. **c** MS images of different *m/z* peaks

imaging (Schwamborn 2012). Multi-modal approaches and details on matrix application methods are included in Chughtai and Heeren (2010). Watrous et al. (2011) cover current applications and future perspectives of MS imaging in biological research.

In this review, we discuss MALDI-based mass spectrometry imaging with a focus on spatial resolution and molecular information content. We describe the methodology and application of a recently developed mass spectrometry imaging method with high resolution in mass ($R = 30,000$) and space (pixel size 3–10 μm).

Critical parameters in mass spectrometry imaging

Mass spectrometry imaging is a highly complex and interdisciplinary analytical technique. This section covers selected fundamental and practical aspects that have a significant effect on the outcome of an MS imaging experiment.

Sample preparation

Sample preparation is probably the most critical step in mass spectrometry imaging. All procedures should be optimized as to retain the native spatial distribution and molecular identity of analyte compounds in the sample as far as possible. Mass spectrometry imaging experiments are typically performed on (thin) tissue sections. However, classical embedding material for sectioning such as 'optimal cutting temperature' compound (OCT) should be avoided if possible. These polymers often result in substantial ion suppression and background signals which can severely interfere with mass spectrometric analysis. Therefore, cryosections of tissue without embedding are used if possible. More delicate samples can be prepared with embedding materials that have been reported to be compatible with mass spectrometry imaging, this includes carboxymethyl cellulose (CMC) (Kawamoto 2003), gelatine (Altelaar et al. 2005), a polymer compound (Strohalm et al. 2011) and tragacanth gum (Brignole-Baudouin et al. 2012).

The second crucial step in sample preparation is the application of matrix which is necessary to desorb and ionize sample components. The matrix needs to interact with the sample (surface) in order to extract analytes from the tissue and incorporate them into matrix crystals. At the same time, spatial integrity of the sample has to be preserved and analyte migration should be limited as far as possible. A number of sample preparation methods have been developed for MALDI imaging. A simple way of matrix application is spraying of a concentrated matrix solution by means of a thin-layer chromatography (TLC) sprayer (Stoeckli et al. 2007b). This method provides

effective analyte incorporation, but can also lead to substantial spatial spreading of analytes if spraying conditions are not carefully controlled. An increasing number of commercial matrix application devices have been developed recently. They include the 'ImagePrep' (Bruker Daltonik, Bremen, Germany), which utilizes 'vibrational vaporization' to generate a spray of matrix droplets (Schuerenberg et al. 2007), and the 'SunCollect' sprayer (SunChrom, Friedrichsdorf, Germany), which employs a pneumatic sprayer. Both systems can achieve matrix crystal sizes below 50 μm in diameter. Spotting devices for MALDI matrix include the 'CHIP-1000' (Shimadzu Corp., Kyoto, Japan), which is based on piezoelectric technology, and a spotter from Labcyte (Sunnyvale, CA, USA), which is based on acoustic droplet deposition (Aerni et al. 2006). These systems provide matrix deposition spots of about 200 μm in diameter. High spatial resolution in MALDI imaging requires matrix crystals which are in the range of the laser spot size, that is the intended pixel size. Therefore, a two-step approach including matrix sublimation and subsequent recrystallization was developed by Bouschen et al. (2010). This method provides homogeneous matrix coverage and allows MALDI imaging at 1–2 μm spatial resolution. Similar approaches were developed by Thomas et al. (2012) and Yang and Caprioli (2011), which were applied to lipids and proteins, respectively. A pneumatic spraying device capable of obtaining matrix crystals below 10 μm was developed by Bouschen et al. (2010).

Irrespective of the matrix application method, a certain level of experience and practice is needed in order to obtain suitable results. Great care should be taken during each step of sample preparation, and experimental parameters should be adapted for each application (sample type and targeted compounds). This includes the choice of matrix which has a significant effect on crystal size and the set of compound classes that can be detected. The first MALDI imaging experiments were performed with 2,5-dihydroxybenzoic acid (DHB), and this matrix is still used in many studies, mainly for lipids and small molecules (Debois et al. 2010; Groseclose et al. 2007; Spengler and Hubert 2002; Spengler et al. 1994). α-Cyano-4-hydroxycinnamic acid (CHCA or HCCA) is also mainly used for small molecules, especially for peptides (Schwartz et al. 2003) and drug compounds (Prideaux et al. 2011; Stoeckli et al. 2007a). Proteins are typically analyzed with sinapinic acid (SA, 3,5-dimethoxy-4-hydroxycinnamic acid) (Grey et al. 2009; Leinweber et al. 2009; Yang and Caprioli 2011). While most MALDI imaging experiments were performed in positive ion mode, an increasing number of studies in negative ion mode has been reported, often using 9-aminoacridine (9AA) as matrix (Shroff et al. 2008; Benabdellah et al. 2009a; Burrell et al. 2007). Matrix compounds that can be used in positive as well as in negative mode include 4-nitroaniline and 1,5-diaminonapthalene (Thomas et al. 2012).

Mass spectral data

An important factor in generating MS images is the 'bin width,'[2] which defines the integration range on the m/z scale for a certain imaged ion signal. Intensity values for pixels in the MS image are calculated by integrating a small m/z window within the corresponding mass spectrum. Intensity values of two peaks are added up if they fall in the same bin. Thus, the bin width has significant influence on the generated MS image and has to be chosen according to the complexity of the sample and the resolution and accuracy of the mass spectral measurement (examples are shown in Figs. 6, 8). Consequently, the choice of the mass analyzer has significant impact on the quality of MS images.

The most widely used detectors for MALDI imaging are time-of-flight (TOF) mass spectrometers. These instruments are sensitive and are available in many (bio)analytical laboratories. They have been employed for a wide range of applications, such as MS imaging of lipids (Benabdellah et al. 2009b; Thomas et al. 2012; Chen et al. 2009), drugs/metabolites (Benabdellah et al. 2009a; Stoeckli et al. 2007a) and peptides/proteins (Stoeckli et al. 2002; Mange et al. 2009; Lemaire et al. 2006, 2007b; Francese et al. 2009; El Ayed et al. 2010; Rohner et al. 2005). Time-of-flight mass spectrometers in reflection mode reach a mass resolving power of up to $R = 30,000$ and mass accuracies better than 5 ppm. However, this performance is only obtained for measurements of homogenized thin-layer samples. In MS imaging experiments, the three-dimensional structure of the sample affects ion flight times and results in significantly lower mass resolution and mass accuracy. Height differences, which cannot be entirely eliminated, lead to inhomogeneity in the acceleration field and thus to a shift in detected flight time (and the corresponding m/z value). Mass accuracy of axial TOF mass spectrometers under tissue imaging conditions is in the range of several tens of ppm if the measurement is controlled carefully. However, mass deviations up to m/z 0.5 are also not uncommon in MS imaging experiments. One way to reduce these detrimental effects are orthogonal TOF systems where the ions are accelerated perpendicularly to the initial extraction direction. These instruments are typically equipped with a quadrupole filter in front of the time-of-flight analyzer (QTOF) to allow MS/MS experiments (Loboda et al. 2000). Mass accuracies reported for MS imaging are in the range of 20–30 ppm

---

[2] This parameter is also described as 'bin size,' 'integration range' or 'mass window,' The term 'bin width' will be used in this work.

(Djidja et al. 2010). Applications of these systems include drug compounds (Stoeckli et al. 2007a), peptides (Djidja et al. 2009; Djidja et al. 2010; Trim et al. 2010) and lipids (Prideaux and Stoeckli 2012; Trim et al. 2008). MALDI–QTOF systems have also been combined with ion mobility spectrometry separation (Stauber et al. 2010; Djidja et al. 2009). This method adds an additional gas-phase separation step (based on the collisional cross section), which can help to resolve the complexity of biological samples.

The highest mass resolving power and mass accuracy are obtained with Fourier transform ion cyclotron resonance (FTICR) mass spectrometers (Marshall and Hendrickson 2002; Amster 1996; Marshall 2000; He et al. 2001; Römpp et al. 2005). These analyzers have the advantage that the cyclotron frequency (and thus the measured m/z value) is independent of the kinetic energy of the ions. This results in mass accuracies of better than 1 ppm which can also be obtained in MS imaging experiments. FTICR mass spectrometers have been used for MS imaging of peptides (Taban et al. 2007) and drug compounds (Cornett et al. 2008). Spatial resolution in these cases was between 200 and 300 μm. Sensitivity was lower than for regular MALDI–TOF instruments. The combination of an FTICR mass spectrometer with a MALDI imaging ion source at a spatial resolution of 7 μm was demonstrated for artificial targets by Koestler et al. (2008).

Development of the orbital trapping mass spectrometer (Orbitrap, Thermo Fisher Scientific GmbH, Bremen, Germany) greatly improved limits of detection (LOD) for accurate mass measurements (Makarov 2000; Makarov et al. 2006). This system is based on the detection of ions trapped in an electrostatic field and does not require a superconducting magnet. Apart from easier handling and lower maintenance costs, this also allows for more efficient ion transmission. Ions are accumulated in a so-called C-trap which is located only centimeters away from the analyzer cell. Orbital trapping mass spectrometers are widely used in bioanalytical applications, typically coupled to liquid chromatography (LC) systems by an electrospray ionization source (ESI). They were also used to image lipids (Landgraf et al. 2009) and peptides (Chen et al. 2010). Orbital trapping mass spectrometers were used for all our measurements which are presented in this review.

Spatial resolution

Spatial resolution in MALDI imaging experiments primarily depends on the size of the laser focus. While the majority of MALDI imaging studies were performed at a spatial resolution between 50 and 200 μm per pixel, there are a number of notable exceptions. As mentioned above, the first MALDI imaging results were obtained at 1 μm pixel size (Spengler et al. 1994; Spengler and Hubert

2002). The obtained MS images showed in all detail the spatial distribution of peptides and matrix compounds (dihydroxybenzoic acid, DHB) in the crystals of a standard MALDI preparation. The same system was used to image cancer cells at 1 μm step size revealing the distribution of several compounds up to m/z 5,000 (Bouschen et al. 2010). A similar optical setup built by Bernhard Spengler was used by Chaurand et al. (2007) to image proteins at 10 μm pixel size. Recently MALDI imaging at 10 μm pixel size using (slightly modified) commercial systems was demonstrated for lipids (Thomas et al. 2012) and proteins (Yang and Caprioli 2011).

The pixel size of the MS image is determined by the distance that the sample is moved between two measurements. This step size is usually chosen in the same range as the laser focus diameter in order to avoid overlapping of analyzed areas. An alternative is to move the sample by less than the focus size resulting in 'oversampling.' If the laser ablates all material of the sample, this method can generate reasonable MS images with a pixel size that is several times smaller than the laser focus size. This was demonstrated for lipids at 15 μm pixel size (Snel and Fuller 2010) and for peptides prepared from cells (Jurchen et al. 2005). It has to be noted that oversampling improves pixel resolution on the cost of sample loss. This is because a large-focus beam has a much lower beam intensity slope at the focus edges than a small-focus beam. The shallow intensity gradient significantly leads to premature sample evaporation outside the ionization zone and thus to a lower overall ion yield.

Another method of obtaining MS image pixels smaller than the laser spot size is the so-called microscope mode (Altelaar et al. 2007; Froesch et al. 2010; Luxembourg et al. 2004). In this case, the laser irradiates an area of 200 μm in diameter and the ions are extracted and detected in a spatially resolved manner. This method can deliver a pixel size of about 4 μm, but practical issues such as detection speed make it difficult to acquire MS imaging data over a larger mass range with this technique (Stauber et al. 2008).

Mass spectrometry imaging with high resolution in mass and space

MS images contain mass spectral and spatial information. Consequently, data need to be acquired in high quality for both dimensions. As described above, high spatial resolution and high mass resolution were achieved from MALDI imaging experiments earlier, but only in separate experiments. We have recently developed a method that for the first time combines a spatial resolution in the low micrometer range and high mass accuracy for the analysis of biological samples. Phospholipids (Römpp et al. 2010a), neuropeptides (Guenther et al. 2011) and drug compounds (Römpp et al. 2011b) were imaged with accurate mass at a

pixel size between 5 and 10 μm. Spatial resolution for tryptic peptides after on-tissue digestion is lower, but 50 μm pixel size was demonstrated for this application (Schober et al. 2012a). In all cases, this method provided a significant improvement in spatial resolution and/or reliability of identification compared to published methods as discussed below.

Methodology

An important aspect in order to obtain high-quality and reproducible results from tissue samples was to systematically evaluate and optimize every step of the analytical workflow for the specific application. This included sample selection, sample preparation, instrumental measurement parameters, but also acquisition, processing and interpretation of data. The following describes general aspects of the workflow which are common to most of our studies. More specific details and additional information are provided below in the individual sections covering the different applications.

Sample preparation

Tissue samples were snap-frozen immediately after the animal was sacrificed and stored at −80 °C. No embedding or fixation was used. Thin sections of tissue with a thickness of 10–20 μm were prepared with a microcryotome (HM 525, Thermo Scientific, Dreieich, Germany) and thaw-mounted on regular microscope glass slides. Conductive coating of glass slides, indium tin oxide (ITO), is not required, but was used in some applications. Tissue sections were covered with matrix by a pneumatic sprayer (Bouschen et al. 2010). 2,5-Dihydroxybenzoic acid (DHB) at a concentrations of 30 mg/mL in acetone/water (0.1 % TFA) 1:1 v/v was used as matrix solution. Matrix crystals in the low micrometer range were obtained with this system. Tissue sections were stained after the MS imaging measurement in order to allow for a detailed analysis of histological features. This included staining with hematoxylin and eosin (H&E), toluidine and Luxol fast blue (Riedelsheimer et al. 2010).

Mass spectrometry imaging

Experiments were performed using a home-built atmospheric pressure scanning microprobe matrix-assisted laser desorption/ionization (AP-SMALDI) imaging source attached to a linear ion trap/Fourier transform orbital trapping mass spectrometer (LTQ Orbitrap Discovery, Thermo Scientific GmbH, Bremen, Germany). The setup of the AP-SMALDI imaging source is described in detail

elsewhere (Koestler et al. 2008). The source works at atmospheric pressure and thus allows analyzing biological samples in their native form without the need for dehydration. A nitrogen laser (wavelength 337 nm) with a repetition rate of 60 Hz was used. The laser beam was focused onto the sample by a centrally bored objective lens. In this system, the optical diameter of the focused laser beam is 8.4 μm (as defined by a decrease in beam intensities at the edges to $1/e^2$ (13.5 %) of its peak intensity). The diameter of the ablation area (which defines the effective spatial resolution) depends on the laser fluence on the sample and is typically adjusted to 5 μm. A detailed characterization of the optical system is described in Guenther et al. (2010). The sample is moved in front of the stationary capillary/lens setup by an x, y, z-stage with a precision better than 1 μm. MS imaging data was acquired with a mass resolving power of 30,000 at m/z 400 in profile mode (i.e. mass peaks were not centroided for data reduction). Ions from 30 laser pulses were accumulated in the linear ion trap for each mass spectrum. Automatic gain control (AGC) was disabled during the measurement, and ion injection time was set to a fixed value (typically 650 ms). Mass accuracy was improved by applying internal calibration using the 'lock mass' feature of the Orbitrap mass spectrometer. The dimer $[2DHB - H_2O + H]^+$, trimer $[3DHB - 2H_2O + NH_4]^+$ and pentamer $[5DHB - 4H_2O + NH_4]^+$ of DHB were typically used as reference masses for this procedure. This resulted in a mass accuracy of better than 2 ppm (RMS) achieved for MS imaging experiments of tissue. Mass spectrometer, laser and sample stage are controlled and synchronized by a microcontroller and home-built software. More details on the instrumental setup and experimental parameters can be found in Römpp et al. (2010a).

Software for image generation

MS images were generated by the software package MIRION (Paschke et al. submitted). The imaging software is able to create ion images from any of the detected m/z values with any selected mass window (bin width). MS images can be generated semiautomatically based on a number of selection parameters such as mass range and pixel coverage. Alternatively selected ion images of a defined m/z value can be generated manually. Up to three different ion images are overlayed in red–green–blue (RGB) images by the software to display different ion species in parallel.

Reporting of MS images and mass spectral data

'Images' in mass spectrometry imaging are constructed in the computer from individual mass spectra. Consequently,

the information content of the resulting image can only be as good as that of the underlying mass spectral data. Therefore, we take extra care to ensure the quality and validity of our reported MS imaging data. If not explicitly stated differently, all data presented in this work adhere to the following rules. Intensity values in selected ion images were normalized to the highest intensity within the image, measured for each ion species separately. MS images do not include any spatial interpolation, smoothing or pixel-wise normalization, in order to allow for an unbiased evaluation. No overlay with optical images is used for MS image presentation. Black-and-white images of selected raw data are usually reported in the supporting information of the original research publications. Step size of the stage movement is identical in x and y direction, that is square pixels are measured and displayed.

The terms 'mass deviation,' 'mass accuracy' and 'maximum mass deviation' are used according to the definition by Zubarev and Mann (2007). All measurements are based on high-resolution mass spectrometry data (mass resolving power $R > 20,000$ @ m/z 700), and images are generated with a bin width of $\Delta m/z = 0.01$. In almost all cases, this proved to be necessary in order to resolve the complexity of biological samples. Mass spectra acquired from single pixels are presented in order to allow an evaluation of the quality of the underlying measurements. Mass accuracy is not (solely) discussed on the basis of selected mass spectra, but is reported as values of the root mean square of m/z deviations across the whole imaging measurement. Accurate mass measurements (RMS < 3 ppm) are used for assignment of imaged compounds. Identification is confirmed by additional MS/MS experiments whenever possible. All these factors are relevant in order to report and evaluate the data in a reliable and comprehensive way.

Phospholipids

Phospholipids are major structural components of all cell membranes and play a crucial role in the cell metabolism of all organisms. Phospholipid derivatives play an important role in signal transduction and are thus of high relevance for numerous pathological processes (Abrass 2004; Lee et al. 2003). Changes in lipid metabolism are major factors in diabetes and cancer (Paradisi et al. 2010; Santos and Schulze 2012). Lipids have been analyzed by mass spectrometry imaging in a number of studies (Sparvero et al. 2010; Jackson et al. 2005; Benabdellah et al. 2009b; Thomas et al. 2012).

The first application of our high-resolution mass spectrometry imaging method in the field of tissue analysis was the analysis of phospholipids in mouse urinary bladder

(Römpp et al. 2010a). A measurement with 10 μm pixel size is shown in Fig. 2a. The MS image shows excellent agreement with classical histological information (after toluidine staining, Fig. 2b). Certain phospholipid signals could be clearly assigned to different tissue regions (all lipids discussed here were detected as potassium adducts). The outer region of the urinary bladder was found to be characterized by the sphingomyelin compound SM (34:1)[3] (m/z 741.5307, Fig. 2a, blue). This histological region could be further subdivided into the adventitial layer, the outermost thin layer as indicated by increased signal intensities of SM (34:1) and the detrusor muscle mainly consisting of smooth muscle tissue.

Following the muscle layer is the loose connective tissue of the lamina propria, characterized by intense signals of m/z 743.5482 (Fig. 2a, red). Colocalization with SM (34:1) displayed in blue results in the magenta color of this region in the RGB overlay. Toward the bladder lumen, a thin layer of subepithelial myofibroblasts was found to be characterized by again high signal intensities of SM (34:1) (Fig. 2a, blue). The high cell densities of both layers were expressed in the stained image (Fig. 2b). The innermost layer of the mucosa is composed of the bladder epithelium (urothelium), indicated by the phosphatidylcholine species PC (34:1) at m/z 798.5410 (Fig. 2a, green). This discussion shows that our MS imaging method can reproduce very detailed histological features, close to cellular resolution. In addition, it also provides highly reliable molecular information.

A mass spectrum acquired from a single 10-μm pixel from the urinary bladder imaging experiments is shown in Fig. 2c. Several peaks are labeled based on accurate mass measurements. Mass deviation of assigned peaks in this spectrum was below or equal to 1 ppm. Mass accuracy as determined over the whole measurement (10965 spectra) was 0.6 ppm (root mean square of all mass deviations) for PC (34:1) at m/z 798.5410. This demonstrates that accurate mass detection is stable over the whole measurement under imaging conditions. This is a prerequisite for reliable identification of compounds and for specific image generation. Another important factor that influences MS image quality is mass resolution. The effect of different bin widths used for image generation is discussed in detail in Römpp et al. (2010a), (Figure S5). MS images with $\Delta m/z = 0.01$ result in complementary spatial intensity distributions of two individual compounds, whereas a bin width of $\Delta m/z = 0.1$ (which is often used in MS imaging

---

[3] Lipids are denoted by the abbreviation for the respective compound class followed by the total number of C atoms and the number of double-bonds in the fatty acid chains. The chain lengths of the individual fatty acid residues and the location of the double-bonds cannot be resolved on the basis of accurate mass. This can be achieved through additional MS/MS measurements.
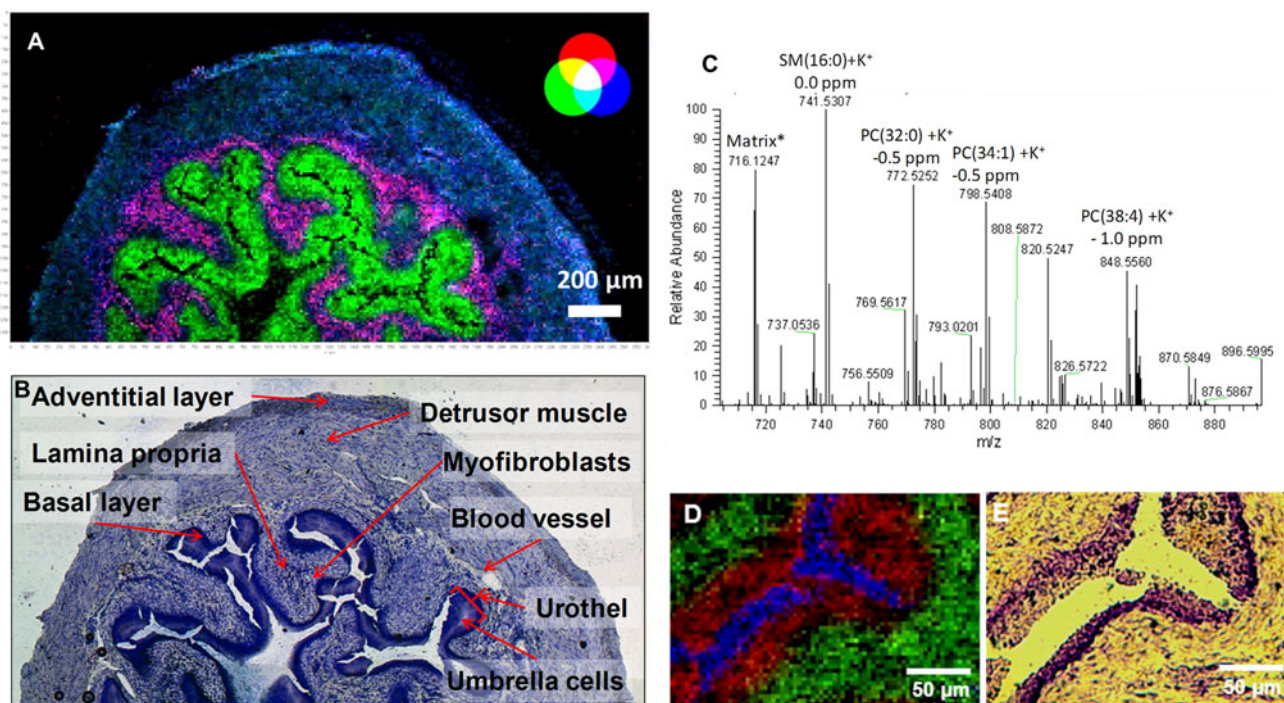
Fig. 2 Mouse urinary bladder **a** MS image, 10 μm pixel size, 260 × 130 pixels, *blue* muscle tissue, SM (34:1), [M + K]$^+$, *m/z* 741.5307, *green* urothelium, PC (34:1), [M + K]$^+$, *m/z* 798.5410, *red* lamina proria, *m/z* 743.5482. **b** Optical image of same tissue section after staining (*toluidine blue*). **c** Mass spectrum acquired from a single 10-μm pixel. **d** MS image, 5 μm pixel size, 260 × 130 pixels (detail of larger measurement): *blue* substrate, Indium cation, *m/z* 114.9039, *red* PC (34:1), [M + K]$^+$, *m/z* 798.5410, *green* SM (34:1), [M + K]$^+$, *m/z* 741.5307. **e** Optical image of same tissue section after staining (*toluidine blue*). Modified from original figure by Römpp et al. (2010a). Copyright © 2010 WILEY–VCH Verlag GmbH & Co. KGaA, Weinheim

experiments) is not able to resolve this difference. This example demonstrates the benefit of high mass resolution and the importance of choosing the correct parameters for image generation. A bin width of $\Delta m/z = 0.01$ is used for all selected ion images shown in this work (except for Fig. 6 where $\Delta m/z = 0.02$ is used).

A second measurement of the same urinary bladder section (adjacent area) was measured with a pixel size of 5 μm. The selected ion images of two phospholipids in a region of two adjacent tissue regions are shown in Fig. 2d. This measurement also shows excellent agreement with histological staining by toluidine (Fig. 2e). The MS image provides sharp separation between the muscular layer [*m/z* 741.5307, SM (34:1), green] and the urothel [*m/z* 798.5410, PC (34:1), red]. These data demonstrate that the effective analytical resolution is indeed in the range of 5 μm.

These results represented the first combination of high-resolution, high-accuracy mass spectrometry with a pixel size in the low micrometer range for mass spectrometry imaging of biological samples. Both features are necessary in order to obtain reliable molecular information from tissue sections on a cellular level. These results also show that phospholipids are highly specific for different cell types and can thus provide detailed histological

information. This information can be used to differentiate and assign features in tissue section which might not be apparent when using classical histological techniques.

Drug compounds

Detection of drug compounds is a major application of mass spectrometry imaging (Prideaux and Stoeckli 2012). The ability for label-free detection of and differentiation between drug compounds and metabolites are its major advantages compared to autoradiography, which is the routine method to investigate the spatial distribution of drug compounds in animal models (Solon et al. 2010). The spatial resolution in MS imaging measurements of drug compounds typically has been in the range of 200–500 μm, which is sufficient to analyze whole body sections (Khatib-Shahidi et al. 2006; Stoeckli et al. 2007a) or individual rat organs (Cornett et al. 2008), but insufficient to resolve detailed features in mouse organs. The highest spatial resolution reported before for drug compounds was 100 μm (Acquadro et al. 2009; Stoeckli et al. 2007a). MS imaging experiments with accurate mass detection for drug compounds were performed at 350 μm spatial resolution (Cornett et al. 2008). Drug compounds are usually detected

in MS/MS mode in order to increase the specificity of the measurement and to prevent interference of matrix cluster ions which are typically abundant in the low mass range (Stoeckli et al. 2007a). The number of compounds that can be detected in one experiment is limited in this approach.

Following the promising results on phospholipids, we investigated the distribution of drug compounds by 'mass spectrometry imaging with high resolution in mass and space (HR^2 MSI)' (Römpp et al. 2011b). The anticancer drug imatinib (a tyrosine kinase inhibitor) was analyzed in mouse kidney at 35 μm pixel size. Selected ion images of phospholipids are shown in Fig. 3a. The distribution of these phospholipids corresponds very well to histological features of the kidney as determined by H&E staining (Fig. 3c). The distribution of the drug compound imatinib in the mouse kidney is shown in Fig. 3b. Imatinib

$([M + H]^+$, m/z 494.2662) is displayed in green, while two phospholipids (red and blue) are included to indicate the histological features of the kidney. Identification and structural characterization of tissue regions, which usually requires examination of the H&E-stained section by a trained histologist, is possible based on the MS imaging data of lipids. This information can be used to determine the exact location of the targeted analyte in the mouse kidney. The colocalization of imatinib (Fig. 3b, green) and PC (40:6) (Fig. 3a, blue) indicates that imatinib is accumulated in the outer stripe of the outer medulla.

A mass spectrum acquired from a single 35-μm pixel is shown in Fig. 3d. The molecular ion peak ($[M + H]^+$) of imatinib was detected with a mass deviation of −0.4 ppm and a mass resolution of $R = 30,000$ in this spectrum. The overall mass accuracy for imatinib in the imaging
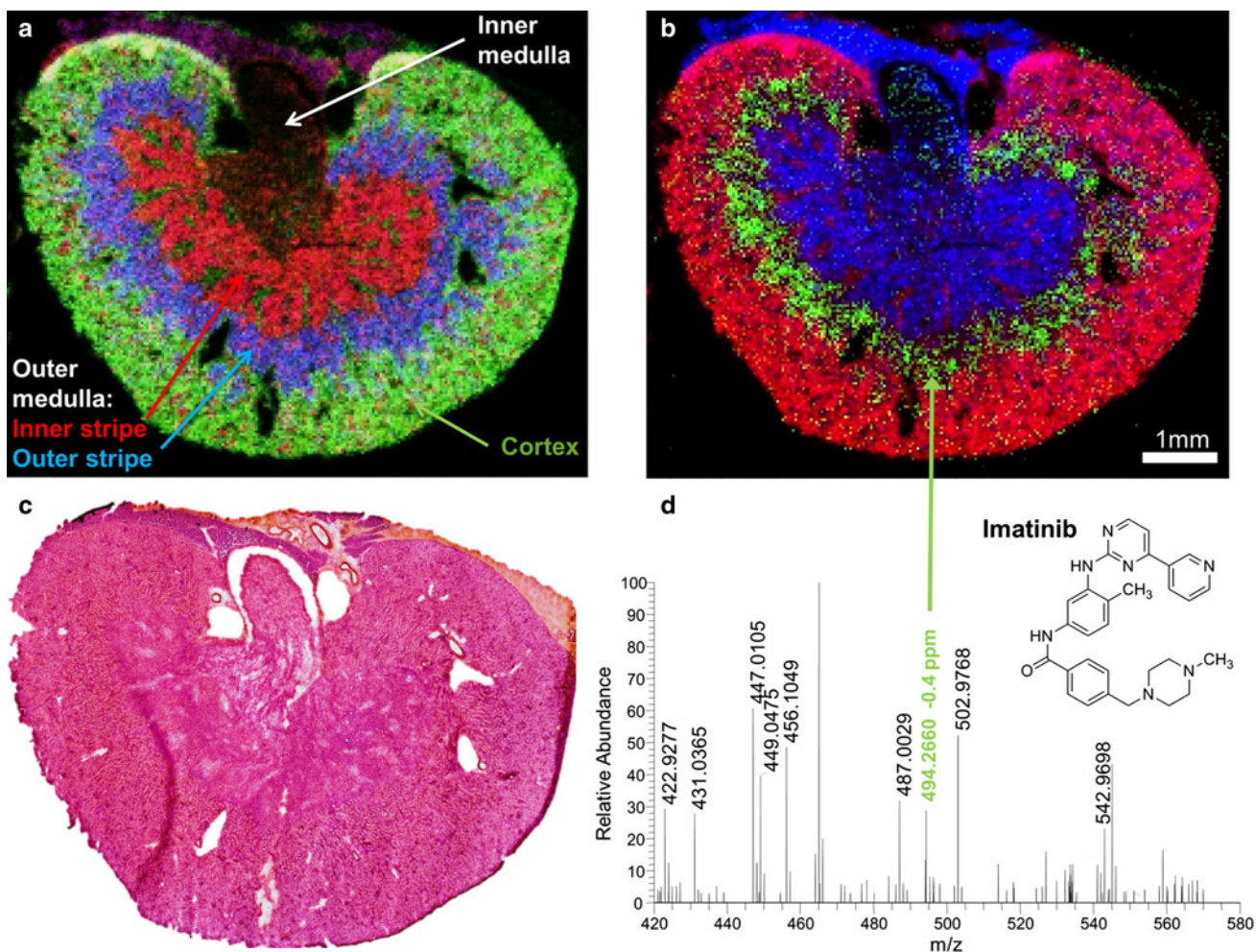

Fig. 3 Mouse kidney **a** overlay of selected ion images: *green* [PC (32:0) + K]$^+$ = 772.5253 cortex, *blue* [PC (40:6) + K]$^+$ = 872.5566 outer stripe outer medulla, *red* [PC (38:5) + K]$^+$ = 846.5410 inner stripe outer medulla, 225 × 150 pixels, 35 μm step size, bin width $\Delta m/z$ = 0.01; **b** overlay of selected ion images: *red* [PC (32:0) + K]$^+$ = 772.5253, *green* imatinib [M + H]$^+$ = 494.2662, *blue* [PC (34:1) + H]$^+$ = 760.5851, 225 × 150 pixels, 35 μm step size, bin width $\Delta m/z$ = 0.01; **c** optical image of the investigated mouse kidney section, H&E stained after MS imaging measurement; **d** single-pixel mass spectrum of the outer stripe outer medulla of the mouse kidney section. Reprinted from Römpp et al. (2011b)

measurement calculated from 5862 individual spectra was 2 ppm (root mean square of mass deviations in all spectra). The identity of imatinib was verified by additional MS/MS experiments, which showed a characteristic fragmentation pattern.

A smaller area of an adjacent mouse kidney section was imaged with 10 μm pixel size in order to investigate the distribution of imatinib in more detail. The resulting MS images again showed excellent agreement with histological features of the mouse kidney and confirmed that imatinib is specifically accumulated in the outer stripe of the outer medulla [see Römpp et al. (2011b) for details]. This can be tentatively associated with a selective accumulation of drug molecules in the proximal tubules. Imatinib was detected with a mass accuracy of 1.8 ppm RMS (calculated from 5816 individual spectra) in this 10 μm measurement.

Mass spectrometry imaging with high resolution in mass and space (HR^2 MSI) provides detailed information on spatial distribution of compounds. The described measurements represented the first mass spectrometric imaging analysis of drug compounds at 10 μm pixel size. This constituted a 10-fold increase in spatial resolution compared to previous studies. At the same time, the measurements provided detailed information on histological features based on the spatial distribution of phospholipids and other endogenous compounds. Correlation of different images allowed for fast and easy interpretation of the drug compound distribution, and areas of accumulation could be directly linked to certain tissue regions.

Neuropeptides

Neuropeptides are important messenger molecules that control a wide range of regulatory functions and processes within an organism. They are formed in vivo by cleavage of precursor proteins and often undergo posttranslational modifications (PTM). These modifications directly affect the biological function of neuropeptides. Investigation of neuropeptides therefore requires specific detection and reliable identification. This can be difficult with histochemical methods as antibodies are not always able to differentiate PTMs. Previous MS imaging approaches for neuropeptide analysis included high spatial resolution (Altelaar et al. 2006, 2007), high mass resolving power and mass accuracy (Taban et al. 2007; Chen et al. 2010) or MS/MS capabilities (Chen et al. 2009; Verhaert et al. 2007; DeKeyser et al. 2007), but these features were never combined in one experiment.

Therefore the aim of our study (Guenther et al. 2011) was to demonstrate that MS imaging of neuropeptides in mammalian tissue is possible with high mass resolution and with MS/MS analysis at cellular resolution. The

pituitary gland is one of the best known neuropeptide-secreting organs in mammals and was therefore chosen for our experiments. It consists of three distinct histological regions, called anterior, posterior and intermediate lobe. Each of these regions has different functions and produces different neuropeptides. In a first experiment, a section of a complete mouse pituitary gland (approximately 1.5 mm × 2.5 mm) was imaged at a pixel size of 10 μm using a mass range of *m/z* 200–4,000. Figure 4 shows the optical image (a) and examples for MS images of neuropeptides (b–d). The distribution of phosphatidylcholine PC (38:4) (shown in green) was used to indicate the overall shape of the pituitary gland. Neuropeptides originating from the same precursor were found to be colocalized. For example, vasopressin and two variants of copeptin, which are all formed from the prohormone AVP-NPII, were detected in the posterior lobe. The neuropeptides POMC 76–85 (γ-MSH), POMC 103–120 (joining peptide), POMC 124–136 (α-MSH) and POMC 141–162 (CLIP) were detected in the intermediate lobe, where the corresponding prehormone POMC is known to be synthesized. In addition, two modifications of α-MSH, the acetylated and diacetylated forms, were detected in this region. This demonstrates that posttranslational modification of neuropeptides can be differentiated with our method. The determined spatial distributions of all detected neuropeptides were in agreement with their expected biological function. In total, 10 neuropeptides were detected in this measurement.

A single-pixel (10 μm) mass spectrum acquired from the intermediate lobe is shown in Fig. 4e. Peptides were identified by comparing their accurate mass with theoretical values for known neuropeptides. A maximum mass tolerance of 2 ppm was used for this procedure. The identity of the neuropeptides was confirmed by additional MS/MS measurements which were obtained in profiling mode from selected areas of the pituitary gland. The identification of all 10 neuropeptides was confirmed by detailed evaluation of product ion peaks [see Guenther et al. (2011) for details]. Furthermore, the spatial distribution of two peptides was investigated by MS/MS in imaging mode at 10 μm spatial resolution. The resulting product ion images were in excellent agreement with the distributions of their peptide precursor ions, confirming their identity and excluding possible analyte interferences.

In an attempt to resolve the fine structure of the pituitary gland, a smaller area covering all three lobes (indicated by a yellow square in Fig. 4b) was imaged at 5 μm pixel size. An overlay of selected ion images of the neuropeptides is shown in Fig. 4f. Diacetyl-α-MSH (POMC 124–136) was found to be located in the intermediate lobe (green). Vasopressin (AVP-NPII) was detected in the center of the posterior lobe (blue). Oxytocin (OT-NPI 20–28) was also
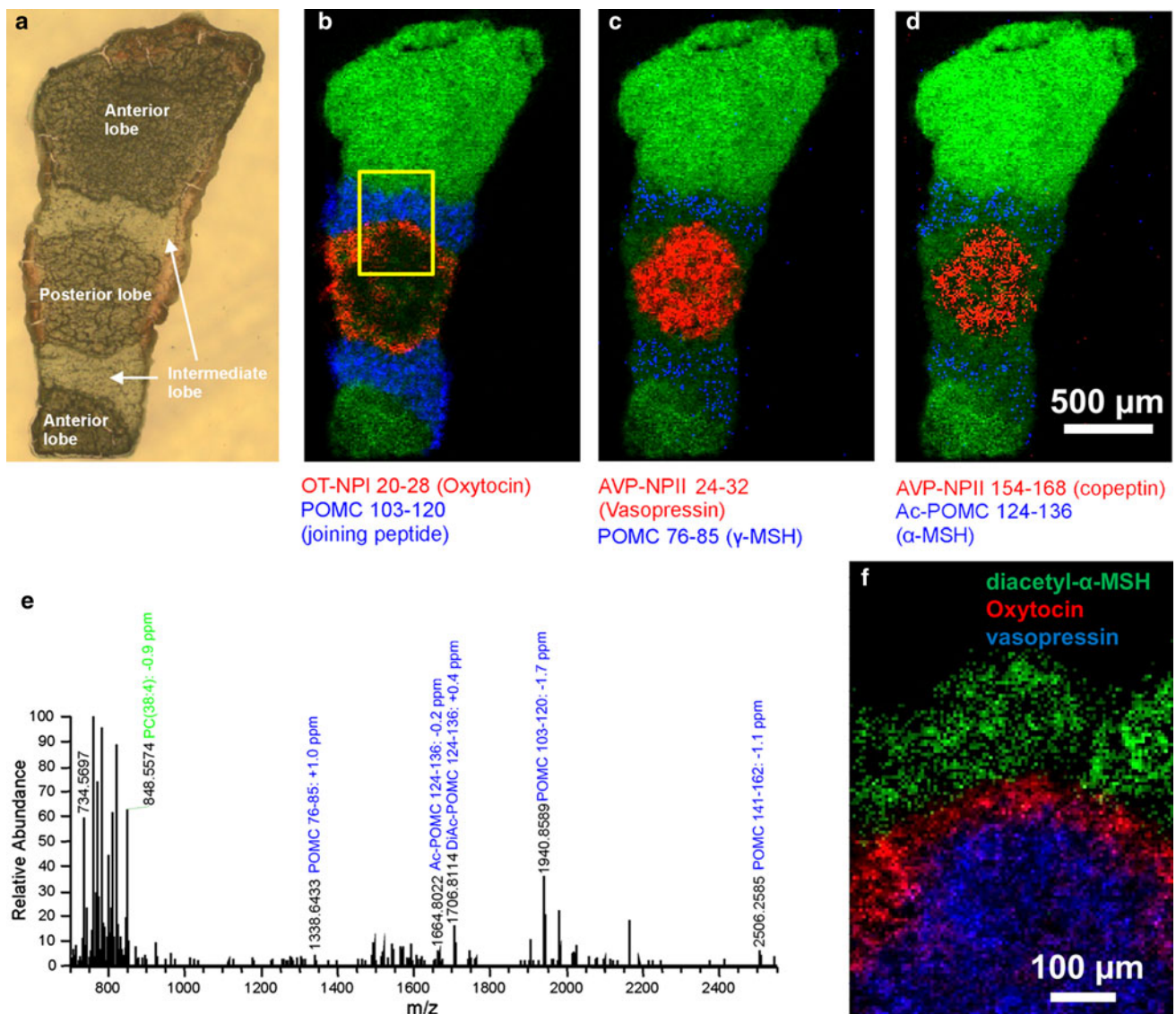
Fig. 4 Mouse pituitary gland. **a** Optical image of mouse pituitary gland tissue section, **b**, **c**, **d** overlay of selected peptide ion images (see label below images) with selected ion image of PC (38:4) (*green*), 155 × 255 pixels, pixel size was 10 μm. **e** Single-pixel mass spectrum from intermediate lobe. **f** Overlay of selected peptide ion images, 100 × 140 pixels. Pixel size 5 μm. *Yellow square* in **b** indicates the location of the measured region. Modified from original figure by Guenther et al. (2011)

present in the posterior lobe, but was primarily detected in the outer region of this lobe. The different distributions of these two peptides are in agreement with the known origin of the corresponding prehormones and can be directly linked to physiological processes on a cellular level [see Guenther et al. (2011) for details].

This study demonstrated that MS imaging of neuropeptides in mammalian tissue is possible at cellular resolution. For the first time, such experiments were performed by combining accurate mass analysis, high mass resolving power and high spatial resolution in one experiment. Peptide sequences were verified by MS/MS experiments, including posttranslational modifications which cannot be differentiated by antibody staining methods.

Proteins (on-tissue tryptic digestion)

Proteins are one of the most studied compound classes in biomedical applications. The analysis of their spatial distributions can provide additional information about their role in physiological and pathological processes. Numerous studies have been published on MS imaging of proteins (Chaurand et al. 2007; Leinweber et al. 2009; Rauser et al. 2010a, b; Shimma et al. 2008; Walch et al. 2008). Spatial resolution for proteins is typically in the range of 100–250 μm. A recent study showed measurements at 10 μm pixel size (Yang and Caprioli 2011). However, protein analysis by MS imaging still faces a number of problems (McDonnell et al. 2010). Direct

analysis under imaging conditions is typically limited to proteins below 30 kDa (Francese et al. 2009), but can be increased in some cases by improved sample preparation techniques (Franck et al. 2010; Leinweber et al. 2009) and/or instrumental modifications (van Remoortere et al. 2010). A major drawback of most studies is that protein signals are not identified, but merely reported as m/z values. This limitation significantly reduces the relevance of reported results for many biomedical applications. Identification of intact proteins from tissue is difficult due to the often limited mass resolution which is insufficient to resolve the complexity of tissue samples. Tandem MS is also of limited use as isolation, and fragmentation efficiency is low for large proteins. Proteins in tissue can be tentatively identified in some cases by additional LC–MS/MS measurements and validated by specific antibodies (Rauser et al. 2010b; Balluff et al. 2010).

An alternative approach is to digest proteins directly on tissue and to image the distribution of the resulting tryptic peptides (Groseclose et al. 2007; Lemaire et al. 2007a). Peptides are easier to detect and identify than the intact proteins, due to their lower molecular weight. This technique has been used for the analysis of tumor samples and other tissue types (Cazares et al. 2009; Djidja et al. 2010). Another advantage of enzymatic digestion is that formalin-fixed paraffin-embedded (FFPE) tissue can be analyzed (Casadonte and Caprioli 2011; Gustafsson et al. 2010; Lemaire et al. 2007a). However, most of these results are still limited to highly abundant proteins (Debois et al. 2010). Typically no more than a few tens of peptides are identified by direct MS/MS measurements (while much more potential peptide peaks are detected). This is due to the limited fragmentation efficiency of singly charged ions, which are produced in MALDI almost exclusively, and to ion suppression effects in the complex matrix of tissue sections.

These limitations can be overcome by a combination of MS imaging with liquid chromatography coupled to mass spectrometry (LC–MS). In this method, one tissue section is analyzed by MS imaging, while an adjacent section is homogenized and analyzed by LC–MS/MS. This approach has recently been applied to lipids (Burnum et al. 2009; Monroe et al. 2008), peptides (Altelaar et al. 2007; Monroe et al. 2008) and proteins (Rauser et al. 2010b; Stauber et al. 2008; Gustafsson et al. 2010). Linking these two modalities is, however, challenging due to the high complexity of the analyzed biological samples (mainly mammalian tissue sections).

The following two sections describe a method for reliable identification of tryptic peptides based on accurate mass measurements followed by an approach to improve spatial resolution.

High mass accuracy MS imaging of tryptic peptides on tissue

The goal of our first study involving tryptic peptides was to improve the reliability of identification by acquiring mass spectra with accurate mass (Schober et al. 2011). In addition, a combination of on-tissue tryptic digestion and complementary LC–MS/MS analysis of the corresponding proteome was applied to increase the number of identified peptides. The highest mass accuracy reported earlier for imaging of tryptic peptides was 30 ppm on a time-of-flight system (Djidja et al. 2010), while most studies reported values in the range of 100 ppm.

In our study, trypsin solution was deposited manually on mouse brain tissue resulting in trypsin spots of about 1 mm diameter (Schober et al. 2011). MS images at a pixel size of 100 μm were acquired from the mouse brain section. In contrast to the other MS imaging experiments discussed in this work, these sections were analyzed with the commercial MALDI source manufactured by Thermo Fisher Scientific (Bremen, Germany). Selected ion images of two peptides are shown in Fig. 5a, b. In the next step, a mouse brain tissue section, adjacent to the one used for MALDI imaging, was analyzed by LC–ESI–MS/MS in order to identify proteins which are present in this tissue. Prior to analysis, this sample was homogenized and fractionated by ultracentrifugation resulting in four subcellular fractions: cytosol, mitochondria/nuclei, endoplasmatic reticulum/golgi and plasma membranes. More than 1,100 peptides corresponding to 500 proteins were identified in this sample. The data from MALDI imaging (tissue section) and from the LC–ESI–MS/MS experiment (homogenate sample) were combined as shown in Fig. 5c, d. In analogy to our previous work (Römpp et al. 2007), a maximum mass deviation of 3 ppm between m/z values of MALDI imaging peaks and masses of peptides identified by LC–ESI–MS/MS was accepted in this study. The two peaks detected by MALDI imaging (Fig. 5c) match with masses of peptides that were identified in the mouse brain tissue by LC–ESI–MS/MS (Fig. 5d). Therefore, the corresponding images were assigned to these two peptides. An unequivocal match of MALDI imaging and LC–ESI–MS/MS data is only possible with a mass accuracy in the low ppm range for both measurement modes, while less accurate measurements would lead to ambiguous assignments. For example, at 30 or 100 ppm mass tolerance, more than one possibility of linking the two measurements existed and would have obstructed an unequivocal interpretation of imaging results [see Schober et al. (2011) for details].

The combination of MALDI imaging and LC–ESI–MS/MS led to the identification of more than 147 peptides corresponding to 101 proteins. More than 75 % of these proteins had a molecular weight of more than 30 kDa and
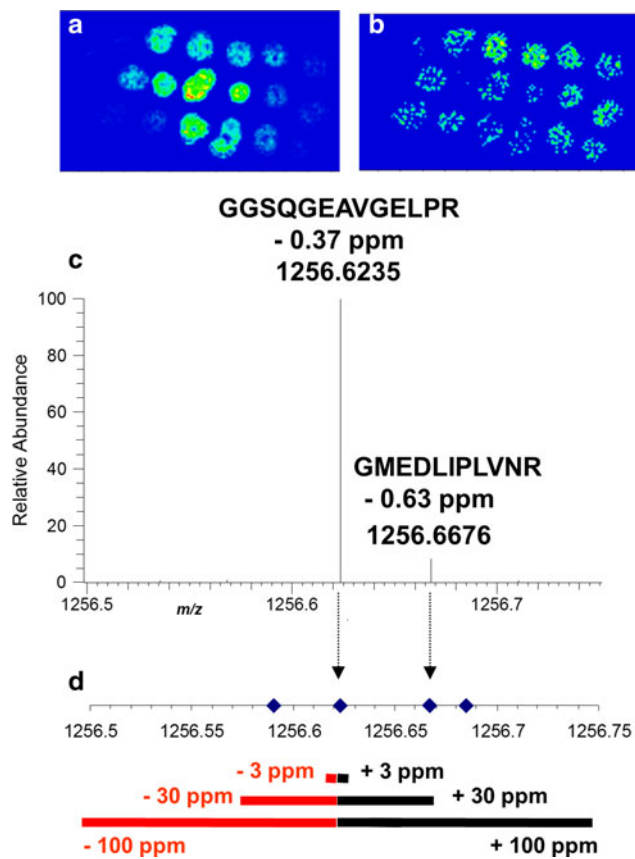
Fig. 5 a, b Selected ion images of two identified peptides with an imaging bin width of $\Delta m/z = 0.01$. **c** Section of the averaged mass spectrum of high mass accuracy MS imaging of mouse brain tissue, containing two identified tryptic peptides. **d** m/z values of all tryptic peptides identified in homogenate LC/ESI–MS/MS measurements in the displayed mass range (m/z 1,256.50–1,256.75). Modified from original figure in Schober et al. (2011). Copyright © 2011 John Wiley & Sons, Ltd

would therefore not be accessible for a top-down approach imaging intact proteins directly on tissue. A total of 24 proteins were detected with two or more peptides and could be considered as reasonable matches. These numbers are in line with comparable studies (Djidja et al. 2009; Gustafsson et al. 2010), but the reliability of identification is significantly higher in our measurements due to accurate mass data.

This study showed that the identification of tryptic peptides without accurate mass and without complementary approaches such as bulk identification methods can easily produce misleading results. In light of these results, the identification results of previous studies have to be considered with care if no independent histochemical confirmation was performed. In particular, in the case of digested tissue sections of high complexity, reliable identification of proteins significantly benefits from high mass accuracy of measurements. This proof-of-concept study was based on low-spatial-resolution

imaging. Results and implications with respect to accurate mass measurements are, however, equally relevant for experiments with smaller trypsin spots as demonstrated in the following section.

Improved spatial resolution for MS imaging of tryptic peptides

The second study on MS imaging of tryptic peptides (Schober et al. 2012a) was focused on increasing the accessible spatial resolution while maintaining the high reliability of the identification step. The critical step in increasing spatial resolution for tryptic peptides is the application of the enzyme solution (usually trypsin). In most of the reported studies, trypsin was deposited in discrete positions by a spotting device (Groseclose et al. 2007; Stauber et al. 2008). Only recently, homogeneous application of trypsin by a spraying device has been reported (Djidja et al. 2010). The spatial resolution of studies reported so far was typically in the range of 200–250 μm. The smallest pixel size for MS imaging of tryptic peptides reported earlier was 150 μm (Stauber et al. 2010).

In our study, trypsin was deposited by a spraying device similar to that used for matrix application (Bouschen et al. 2010). All parameters of sample preparation were carefully optimized (Schober et al. 2012a). Trypsin was deposited in several aliquots (of 3 μL each) in intervals of 15 min, preventing excessive accumulation of liquid on the tissue. The sample was placed in an incubator (37 °C, 100 % relative humidity) between spraying cycles and was incubated overnight after the last trypsin deposition. Another important factor is the employed buffer solution, NH_4HCO_3, which proved to be compatible with subsequent matrix application. We also used a trypsin concentration that was twice as high as in most published studies. The resulting tryptic peptides in a mouse brain section were analyzed by mass spectrometry imaging at 50 μm pixel size. Peptides were identified by comparison with LC–ESI–MS/MS as described above [see Schober et al. (2011)]. One of the first measurements using this new approach is shown in Fig. 6. The mass spectrum acquired from a single 50-μm pixel shows two peaks at nominal mass m/z 726 (Fig. 6a). The myelin peptide HGFLPR (theoretical m/z 726.4046) was detected with a mass deviation of −0.28 ppm and a mass resolution of $R = 24,000$ in this spectrum. The overall mass accuracy for this peptide in the imaging measurement calculated from more than 500 individual spectra was 1.0 ppm (root mean square of all mass deviations). Another signal at the same nominal mass was detected at $m/z = 726.5114$ and was discriminated from the myelin peptide signal. This second peak was identified as an isotopologue peak of the ammonium adduct of the lipid phosphatidylserine PS (30:0) (theoretical

Fig. 6 Mouse brain (*coronal section*) after on-tissue tryptic digestion. **a** Mass spectrum from a single 50-μm pixel. **b** Optical image of adjacent section after staining for myelin (*Luxol fast blue*) **c**, **d**, **e** MS images, 50 μm pixel size, 92×128 pixels: **c** selected ion image of $m/z = 726.40$–726.41 corresponding to myelin peptide. **d** Selected ion image of $m/z = 726.40$–726.60. **e** Selected ion image of $m/z = 726.51$–726.52 corresponding to lipid isotopologue peak. Details on method can be found in Schober et al. (2012a)
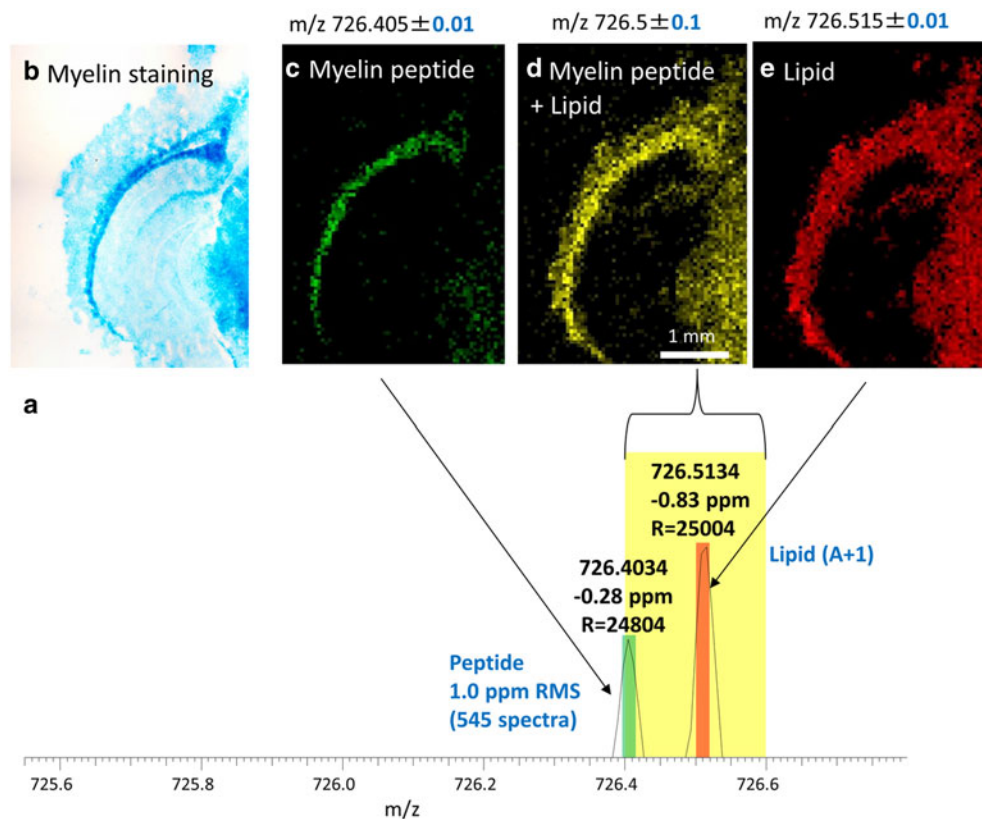
m/z 726.5128). Fig. 6d shows a selected ion image generated with a bin width of $\Delta m/z = 0.2$. In this image, no differentiation between the peptide and the lipid isotopologue was possible; the myelin peptide signal was masked by the lipid isotopologue. Figure 6c, e show selected ion images generated with a bin width of $\Delta m/z = 0.02$ for the myelin peptide and the lipid isotopologue, respectively. In this representation, both analyte distributions were clearly resolved.

The myelin peptide shows a well-defined distribution with high intensities in the *corpus callosum* area of the mouse brain which is in accordance with its physiological function (Sidman 2011). Figure 6b shows the optical image of an adjacent mouse brain section after staining of the myelin sheath (Luxol fast blue). The myelin distributions in the MS image and the histological staining show excellent correlation. This confirms that the spatial distribution of myelin was preserved and no substantial migration of tryptic peptides occurred during the digestion process.

A similar measurement with a higher number of identified peptides is discussed in Schober et al. (2012a). In total, 9 peptides corresponding to myelin and 19 peptides corresponding to other proteins were identified and imaged. All myelin peptides showed well-defined distributions which were highly correlated with each other. The number of identified peptides in this work is in the same range as that of studies reported in the literature (Groseclose et al.

2007; Franck et al. 2009; Shimma et al. 2008), but was obtained at significantly smaller pixel size. Peptides were also identified with a very low mass tolerance of 3 ppm and thus with higher confidence.

These measurements represented the first MS imaging experiment of tryptic peptides with a spatial resolution of 50 μm. The small pixel size shown here cannot be achieved with spotting devices since the size of individual droplets and thus the resulting trypsin spots are too large. Diffusion processes within these trypsin spots on tissue lead to unwanted spreading of peptides. The homogeneous application of trypsin by a spraying device can overcome this problem if spraying conditions such as flow rate, distance and buffer solution are carefully controlled. As for all MS imaging experiments, sample preparation and instrumental parameters have to balance analytical sensitivity and spatial resolution. The experiments in this study were optimized for ultimate spatial resolution. Exact conditions need to be optimized for each tissue type and targeted application.

The obtained results represented a significant improvement over previously reported methods in terms of image quality for tryptic peptides. The improved spatial resolution made smaller histological features accessible. High mass resolving power improved the specificity of the spatial distribution information by reducing interferences with neighboring peaks. Accurate mass allowed for reliable identification of tryptic peptides. Each of these factors was

found to be critical in order to obtain reliable information on biologically relevant compounds. The capabilities of the method were demonstrated in a proof-of-concept study on mouse brain tissue.

Current experiments demonstrate that comparable results in terms of reliable identification can also be obtained from clinical tissue samples. Newest developments also indicate that the number of identified peptides can be significantly increased and that spatial resolution can most likely be further improved.

Single-cell MALDI imaging

Cell cultures are a common model system in biological and biomedical research. The influence of pathogenic and/or environmental factors can be studied under controlled conditions. Metabolic studies in cell cultures are usually based on the analysis of bulk samples. The analysis of individual cells would instead provide much more specific and informative data. Previous attempts to use MS imaging for this application faced a number of problems. Time-of-flight secondary ion mass spectrometry (TOF-SIMS) offers sub-micrometer spatial resolution and is able to image the spatial distribution of metabolites inside single cells (Colliver et al. 1997; Ostrowski et al. 2004). However, TOF-SIMS in single-cell analysis is typically limited in mass range to $m/z < 500$, and detected analytes can often not be identified (Szakal et al. 2011). This is due to severe fragmentation of analyte ions and limited MS/MS capabilities in imaging mode. MALDI imaging, in contrast to that, offers higher mass range and higher mass resolution. However, direct analysis of single cells with this method resulted in only one pixel per cell due to the limited spatial resolution of 40–50 μm in reported studies (Miura et al. 2010; Zimmerman et al. 2011).

Based on the instrumentation and methodology described above, we developed a dedicated workflow for imaging metabolite distribution in single cells (Schober et al. 2012b). Sample preparation is a critical step in obtaining useful results in mass spectrometry imaging, especially at high spatial resolution. Fixation methods with ethanol or formaldehyde resulted in the loss of the cells during sample preparation. The best results for analysis with MALDI MS imaging were obtained by fixation of cells with glutaraldehyde. Experimental details such as temperature of solutions, buffer concentration and incubation times proved to be critical and were carefully optimized. After fixation, cells were stained with 3,3′ dihexyloxacarbocyanine iodide [DIOC$_6$(3)], which is a fluorescence dye that stains cell membranes (Invitrogen 2011). After matrix application, samples were measured with our AP-SMALDI ion source on an 'Exactive Orbitrap' mass spectrometer (Thermo

Fisher Scientific GmbH, Bremen, Germany). This system provided improved sensitivity and mass resolution ($R = 100,000$ @ m/z 200) compared to the previously used 'LTQ Orbitrap.'

The images of two individual HeLa cells are shown in Fig. 7. The signal of DIOC$_6$(3) in optical fluorescence mode (wavelength $\lambda = 501$ nm, Fig. 7a) and MS imaging mode (selected ion image of m/z 445.285, Fig. 7b) show very good correlation. The shape of the cells is clearly visible in the MS image, and their extensions of only a few micrometers in diameter are detectable. This implies that the spatial structure of the cells was not affected significantly by matrix application and the measurement procedure. Figure 7c, d show selected ion images of two phospholipids. The (sodium adducts of) phosphatidylcholines PC (16:0/16:1) and PC (16:0/18:1) were detected primarily in the center of the cell where higher concentrations of membranes are expected. The fatty acid chain length of these two phospholipids was determined by additional MS/MS experiments [see Schober et al. (2012b) for details].

A mass spectrum acquired from a single 7-μm pixel is shown Fig. 7e. Numerous phospholipids such as phosphatidylcholine (PC), sphingomyelin (SM), phosphatidylserine (PS), as well as di- (DG) and triglycerides (TG) were found in the mass range m/z 620–810. As in all our studies, the imaged compounds were detected with accurate mass (better than 3 ppm RMS for the complete image) and therefore allow reliable substance identification. In addition to phospholipids, smaller metabolites such as nucleic acids, amino acids as well as cholesterol were identified in the lower mass range [see Schober et al. (2012b)]. A broad metabolic profile could thus be acquired from a defined area of the cell with high confidence. Alternatively, several spectra acquired from one cell can be combined in order to obtain better statistics for quantitative analysis.

Current experiments focus on the mass range of phospholipids. Invasion mechanisms of pathogens are known to lead to changes in the lipid pattern through enzymatic degradation (Vazquez-Boland et al. 2001). These effects can be investigated with high molecular specificity in single cells at different stages of the infection process with the methodology described here. Another application that is currently evaluated is monitoring the differentiation of stem cells on a molecular level. In general, our method can be used for a detailed investigation of metabolic changes in single cells and can provide more detailed and/or more reliable information than previous MS imaging approaches.

Analysis of lung carcinoma tissue

We typically test our methodology with mouse brain tissue as this is a widely used model system for MS imaging. The
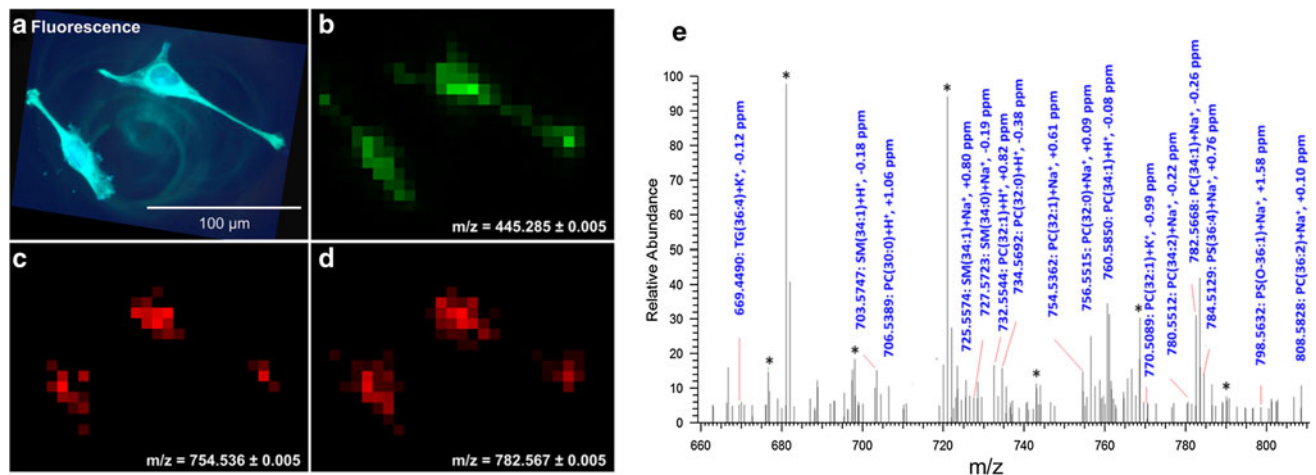
Fig. 7 HeLa cells on ITO-coated glass slide. **a** Optical fluorescence of DIOC6(3)-stained HeLa cells ($\lambda = 501$ nm). **b**, **c**, **d** MALDI imaging, 7 μm pixel size, 28 × 21 pixels (detail of larger measurement): **b** selected ion image of staining agent DIOC6(3), $[M]^+$, **c** selected ion image of phosphatidylcholine PC (32:1), $[M + Na]^+$ and **d** selected ion image of PC (34:1), $[M + Na]^+$. **e** Single-pixel mass spectrum (7 μm) acquired from the region of cell nucleus. Reprinted with permission from (Schober et al. 2012b). Copyright 2012 American Chemical Society

molecular composition of this tissue is well known, and extensive histological information is available in brain atlas resources (Sidman 2011; Hochheiser and Yanowitz 2007). Once a certain method is optimized, it is applied to more relevant samples including clinical tissue sections. An example that was first shown in a conference presentation (Römpp et al. 2011a) is the analysis of a human non-small-cell lung carcinoma that was induced into a severe combined immunodeficiency (SCID) mouse model (Fig. 8). This tissue section was imaged at 10 μm pixel size. MS image analysis (Fig. 8a) shows excellent correlation with the different regions within the cancerous tissue that were identified by the pathologist in the H&E staining (Fig. 8b). Cerebroside Cer (42:2) (Fig. 8a, green) was found to be almost exclusively present in the connective tissue of this section. The tumor region can be further differentiated in the invading tumor edge with high signal intensities of phosphatidylcholine PC (32:1) (Fig. 8a, blue) and the ischemic tumor region that was characterized by high signal intensities of phosphatidylcholine PC (40:6) (Fig. 8a, red). Purple color results from colocalization of PC (32:1) (blue) and PC (40:6) (red). Multiple other lipid species were detected and identified for each tissue region in addition to the examples shown here. Figure 8c shows the distribution of lyso-phosphatidylcholine LPC (16:0) (green), primarily localized in the area of the tumor that was identified as necrotic zone. Lyso-lipids are degradation products of lipids and are therefore expected in areas where cell degradation occurs. This is another example where our method provides more insights about the molecular information that is not directly accessible by classical histological methods. This approach can be applied to

investigate the molecular processes in tumorigenesis and to differentiate tumor states.

Lipids in this measurement were identified by accurate mass data. As demonstrated above for tryptic peptides (Fig. 6), the bin width used for image generation significantly affects the result of an MS imaging experiment. Generating MS images with a bin width of $m/z = 0.1$, as common for many MALDI–TOF measurements, would result in the distribution shown in Fig. 8d. However, the healthy and tumor tissue regions can only be differentiated by using a bin width of $\Delta m/z = 0.01$ (Fig. 8e, f). These black-and-white images represent the raw data acquired from the mass spectrometer without applying any processing steps. Overlay of these two signals shows very sharp separation between (healthy) connective tissue and the tumor region (Fig. 8g). Similar effects were observed for nearly all signals in the lipid mass region. Consequently, the reliable characterization of complex samples such as mammalian tissue sections by mass spectrometry imaging greatly benefits from the use of high-resolution mass spectrometry.

MALDI imaging at 3 μm pixel size

In an attempt to further improve the accessible spatial resolution of MALDI imaging, the lateral ventricle region of a coronal mouse brain section was imaged with 3 μm pixel size. The MS image of this experiment, which was included in a conference presentation (Römpp et al. 2010b), is shown in Fig. 9a. The selected ion image of phosphatidylcholine PC (38:4) shows the detailed structure

Fig. 8 Human non-small-cell lung carcinoma that was induced into a severe combined immunodeficiency (SCID) mouse model. **a** MS image, 10 μm pixel size, 185 × 185 pixels, *red* sphingomyelin SM (36:1), *m/z* 769.5620, *green* cerebroside Cer (42:2), [M + K]⁺, *m/z* 848.6376, *blue* phosphatidylcholine PC (36:4), [M + K]⁺, *m/z* 820.52531. **b** H&E staining after measurement. **c** MS image, 10 μm pixel size, 185 × 185 pixels, *green* lyso-phosphatidylcholine LPC (16:1), [M + H]⁺, *m/z* 496.3397, *red* phosphatidylcholine PC (38:6) [M + K]⁺, *m/z* 844.5253. **d**, **e**, **g** Selected ion images generated with different settings for image generation as indicated in Figure
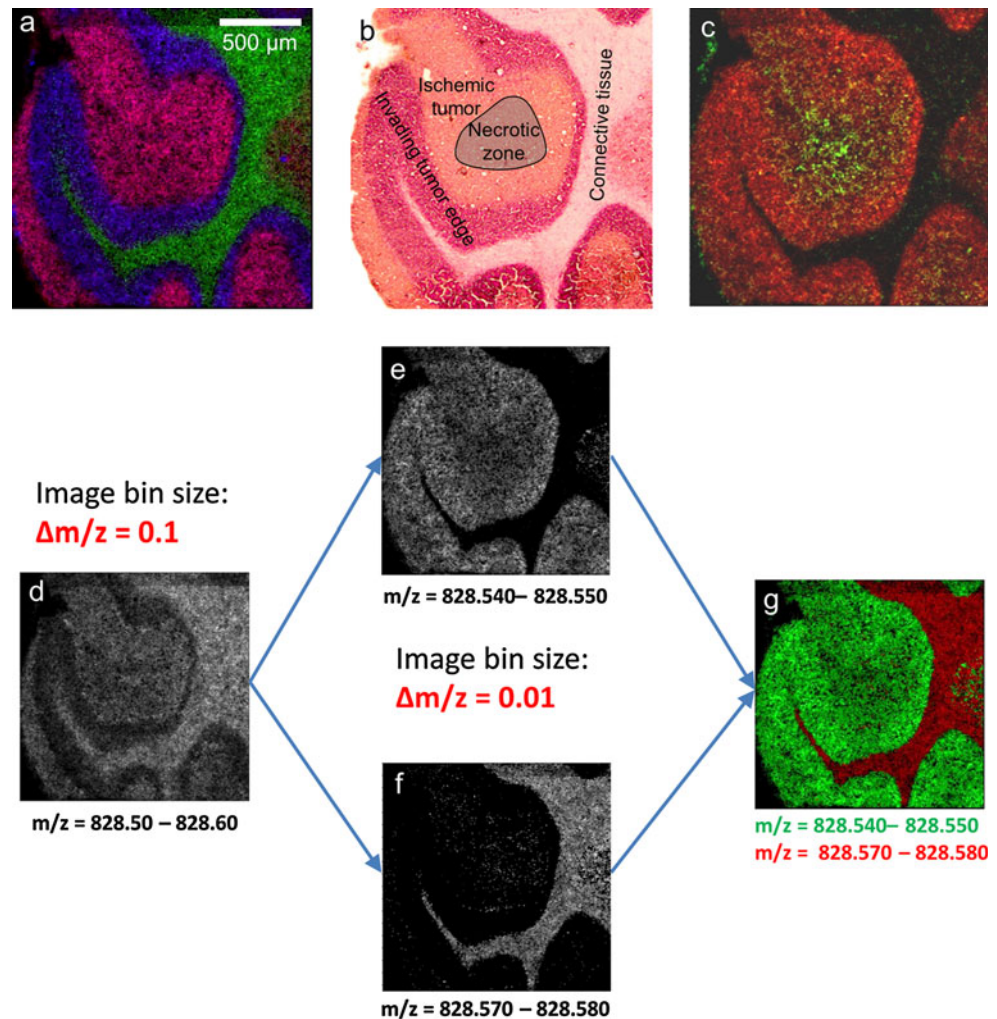
of the choroid plexus (green), while the surrounding tissue is characterized by high intensities of phosphatidylcholine PC (34:1). The optical image of the tissue sample prior to MS analysis is shown in Fig. 9b. The poor quality of the optical image is due to the fact that the sample is completely consumed under these highly focused laser conditions, and subsequent staining of tissue was therefore not possible. The quality of the mass spectral data is, however, not significantly affected by the reduction in pixel size. A mass spectrum acquired from a single pixel (corresponding to 3 × 3 μm² tissue area) is shown in Fig. 9c. Phospholipids in this mass spectrum were detected with a mass deviation of <2 ppm and a mass resolution of about $R = 20{,}000$. Lower signal intensities make recalibration based on matrix cluster signals slightly more challenging in this experiment. These measurements demonstrate that under slight oversampling conditions (at an ablation spot diameter of 5 μm in diameter) still high-quality mass spectral data can be obtained in high-resolution AP-SMALDI imaging and that there is still potential for a further increase in spatial resolution.

Spatial resolution and measurement speed

It is often argued that imaging at high spatial resolution takes too much time. This might be true if two experiments of the same measurement area are compared. But high spatial resolution imaging is typically targeted at smaller structural features which would not be resolved otherwise. Therefore, the spatial resolution (pixel size) of an experiment should be adjusted according to the structure of interest. The speed of our method of about 1 s per pixel is comparable to that of other mass spectrometry imaging systems. Recent experiments indicate that significant increase in speed can be obtained (with almost constant mass accuracy and moderately lower mass resolution). At present, our method already provides reliable MS imaging measurements at different spatial resolution settings as demonstrated in Fig. 10. All three MS images show detailed histological features (at different spatial scales). Figure 10a shows the phospholipid spatial distribution in mouse brain (coronal section) at 5 μm pixel size. The structure of the putamen and the corpus callosum (upper right) are clearly visible. Figure 10b shows a horizontal
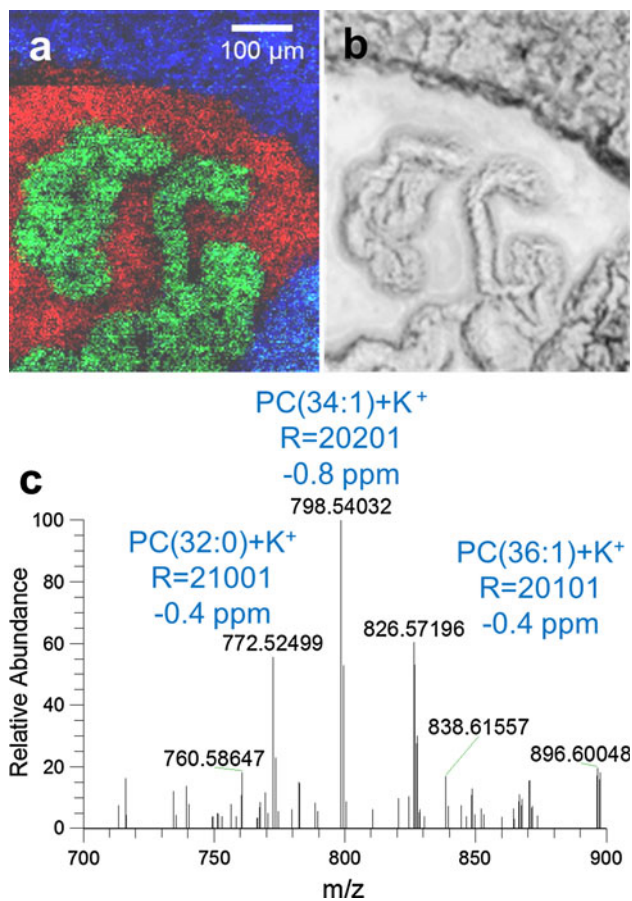
Fig. 9 Lateral ventricle region of mouse brain (coronal section). **a** MS image, 3 μm pixel size, 170 × 300 pixels, *green* phosphatidylcholine PC (38:4), [M + K]$^+$, *m/z* 848.5566. *blue* phosphatidylcholine PC (34:1), [M + K]$^+$, *m/z* 798.5410, *red* background signal from ITO-coated glass slide. **b** Optical image of imaged area before measurement. **c** Mass spectrum acquired from a single 3-μm pixel

section of mouse brain at 50 μm pixel size. The two imaged phospholipids show detailed features in the corpus callosum, striatum and cerebellum region. Figure 10c shows a measurement of the intestinal tract of a whole body rat section at 200 μm pixel size. A phospholipid (red) that provides histological information can be directly used to indicate the localization of a drug compound (green) [see Römpp et al. (2011b) for details]. A useful approach for balancing measurement time and spatial information is to scan a larger area with lower spatial resolution in order to identify areas of interest. These areas can then be scanned with higher spatial resolution in order to investigate the detailed distribution of analytes.

Measurement speed is obviously an important factor when comparing quantitative differences between two biological conditions. In this case, biologically relevant results can only be obtained if the experiment is repeated with several samples (biological replicates). Consequently, higher speed allows for a higher number of measurements and thus provides more reliable results. Another approach is the detailed molecular analysis of a (tissue) sample without prior knowledge. In such an untargeted approach, data analysis and interpretation can be much more time-consuming than the actual measurement itself. In this case, specificity and sensitivity of the measurement is of highest priority and measurement speed is of less importance.

Data analysis: imzML—a common data format for MS imaging

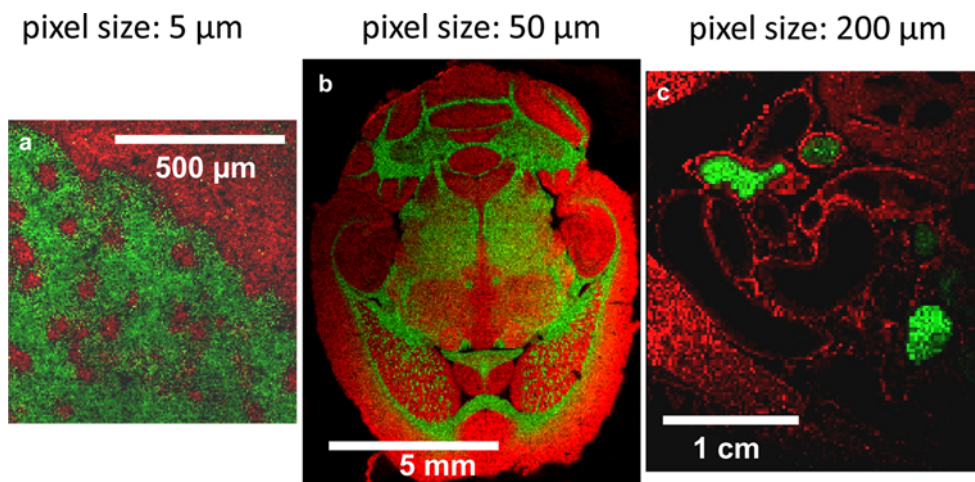Mass spectrometry imaging produces large and complex data sets, and thus efficient strategies for processing and

Fig. 10 MS images of phospholipids in tissue sections at different pixel size settings. **a** Mouse brain (coronal section), pixel size 5 μm, 170 × 170 pixels. **b** mouse brain (*horizontal section*), pixel size 50 μm, 207 × 260 pixels. **c** Intestinal tract of rat (*part of whole body section*), pixel size 200 μm, 128 × 150 pixels

analyzing are essential. A common data format for the flexible exchange and processing of mass spectrometry imaging data was developed within the EU joint project COMPUTIS (www.computis.org). The data format is in part based on the HUPO-PSI format mzML (Martens et al. 2011) and was thus called imzML for 'imaging mzML.' The concept of imzML and application examples are summarized in Schramm et al. (2012). Additional information and all technical details necessary to implement imzML are provided in a book chapter (Römpp et al. 2010c) and on the Web site www.imzml.org.

MS imaging data in imzML format are divided into two separate files. Metadata (e.g. instrumental parameters and sample details) are stored in an XML file. Information in this file is organized in a controlled vocabulary in order to avoid ambiguities (Smith et al. 2007). Mass spectra are stored in a separate binary file in order to ensure efficient data storage. The XML structure in combination with the controlled vocabulary ensures that the data format can be easily adapted to new instrumentation and experimental strategies.

Data sets from more than 10 different MS imaging platforms have been converted into imzML so far. Examples shown in Fig. 11 include data from matrix-assisted laser desorption/ionization (MALDI) as well as desorption electrospray ionization (DESI) and secondary ion mass spectrometry (SIMS). A growing number of processing options are available for the imzML format. The lower part of Fig. 11 shows software tools which were developed by COMPUTIS partners. imzML can also be employed for processing data with different tools sequentially as demonstrated in Schramm et al. (2012). Additional examples of imzML conversion and processing options are displayed in the 'imzML gallery' on www.imzml.org. imzML-based software was also used to process data from our high-resolution mass spectrometry imaging method. While the small pixel size is not a problem, some software tools need to be adapted to handle high mass resolution data (i.e. to generate MS images with a narrow bin width of $\Delta m/z = 0.01$).

imzML can also be used to compare data from different instrument platforms. Options for data processing (e.g. binning, normalization) and visualization (e.g. interpolation options, color schemes) vary strongly between different MS imaging software tools and can make a direct comparison of data difficult. This problem can be avoided if all data sets are converted to imzML and the data are displayed with identical parameters of one software tool [see Schramm et al. (2012) for details].

The concept of imzML is also actively supported by major vendors of MS imaging instrumentation including Thermo Fisher Scientific (Bremen, Germany), Waters
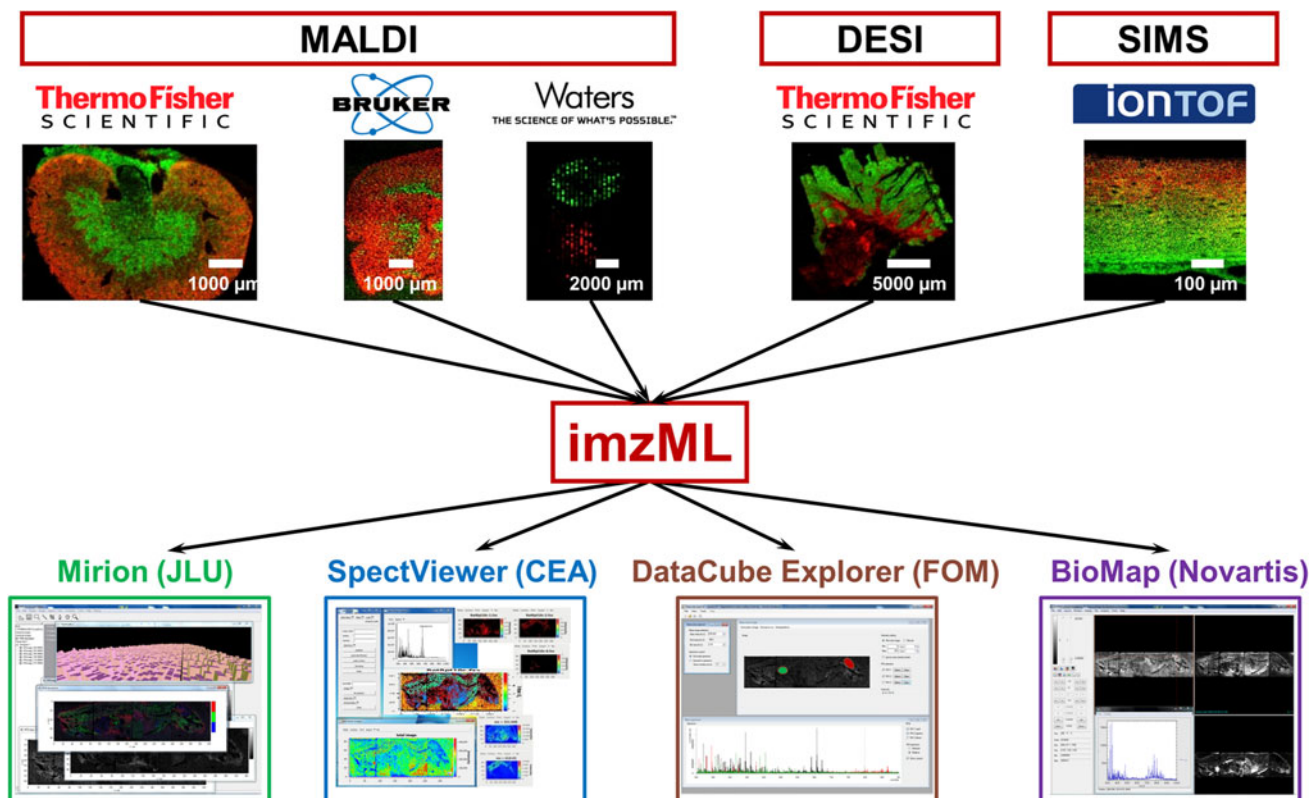

Fig. 11 Combination of data from different MS imaging platforms and software tools on the basis of the common data format imzML. See Schramm et al. (2012) for details

Corporation (Manchester, UK) and Bruker Daltonik (Bremen, Germany). An updated list of available tools and workflows can be found on the imzML Web site. This also includes the first commercial software tools, which are compatible with imzML, from Imabiotech (2012) and PREMIERBiosoft (2012).

imzML provides more flexibility in data processing as the user is no more limited to proprietary software but can choose the processing option that best fits the purpose. Data can also easily be shared between collaborators as several of the software tools are freely available. Measurement results can be provided to partners in biological or clinical laboratories without the loss of information (which is the case when sharing only the images). Finally, a common data format provides more transparency in reporting MS imaging results. Consequently, imzML can facilitate everyday work with MS imaging data.

Conclusion and perspective

The results presented above demonstrate that mass spectrometry imaging with high molecular specificity is possible at or close to cellular dimensions. Lipids, (neuro)peptides and drug compounds were imaged in a wide range of biological samples at a spatial resolution of 5–10 μm. A measurement of mouse urinary bladder at 5 μm step size showed pixel-sharp separation between tissue regions. A drug compound (imatinib) was imaged in mouse kidney at 10 μm pixel size. Correlation with spatial distributions of (simultaneously detected) phospholipids allowed to directly link areas of imatinib accumulation to histological structures. More than 10 neuropeptides were imaged at 5 and 10 μm pixel size in mouse pituitary gland. Peptide identification by accurate mass was confirmed by additional MS/MS imaging experiments.

On-tissue digestion was employed for the analysis of proteins. Tryptic peptides were imaged for the first time with accurate mass and identified by complementary LC–ESI–MS/MS measurements of an adjacent tissue section. This approach significantly increased both the reliability and the number of peptide identifications. In subsequent experiments, the spatial resolution for tryptic peptides was improved to 50 μm while maintaining the high molecular specificity. This was achieved by applying trypsin with a spraying device.

A dedicated sample preparation protocol was established for the analysis of cell cultures. Phospholipids and smaller metabolites such as amino acids and nucleic acids were imaged in single cells. A full metabolic profile was obtained from a single pixel of 7×7 μm^2.

The feasibility of obtaining high-quality mass spectrometry imaging data from clinically relevant tissue was demonstrated by the analysis of lung carcinoma tissue. The highest spatial resolution of a MALDI imaging experiment of tissue so far was obtained by analyzing a mouse brain section at 3 μm pixel size.

MS image analysis for all these experiments showed excellent correlation with histological evaluation. In addition, it provided highly specific molecular information. In many cases, components of very similar mass ($\Delta m/z < 0.1$) showed distinctly different spatial distributions. This demonstrated the need for accurate mass determination in order to obtain reliable information from MS imaging experiments of biological samples. The ability to combine high mass resolution and accuracy with a high spatial resolution in the low micrometer range is a unique feature of the presented method.

Each of these studies represented a significant improvement in spatial resolution and/or reliability of identification compared to studies reported earlier. These methodological improvements were made possible by the development of an integrated workflow that is optimized for 'mass spectrometry imaging with high resolution in mass and space.' The experiments presented above were not merely the application of one method to different samples, but involved new experimental approaches for each study. For example, sample preparation was carefully adjusted for each application. This was especially important for the analysis of single cells and the detection of tryptic peptides, but also for the analysis of highly water-soluble analytes such as neuropeptides and drug compounds.

While small pixel size is not necessarily a prerequisite for high-quality MS imaging, higher mass accuracy and mass resolution will always result in more reliable data. The high complexity of biological samples inevitably leads to multiple peaks for each nominal mass. High mass accuracy significantly improves the reliability of identification as demonstrated in the examples above. This is even more important when different MS methods are combined as shown for the example of tryptic peptides. Therefore, MS imaging experiments should always be designed as to deliver the highest mass accuracy and mass resolution possible (for a given instrumental setup). More frequent mass calibration steps, internal standards and/or postrun recalibration can be used to achieve this goal.

Up to now, we have applied our mass spectrometry imaging method to a wide variety of applications. Targeted compound classes included lipids, amino acids, peptides, proteins, nucleic acids, carboxylic acids and carbohydrates. In addition to the examples discussed above, we have analyzed several sample types including muscle, testis, spinal disk as well as adrenal gland tissue originating from mouse, rat, pig or cow. In these experiments 'mass spectrometry imaging with high resolution in mass and space' proved to be a versatile and robust method for the highly detailed analysis of biological samples.

A major focus of our current and future studies is the analysis of clinical tissue samples. Several types of human tumor biopsies are currently being analyzed. Sets of carefully selected samples will be analyzed in close collaboration with clinical partners. On the methodological side, the current activities are aimed at further improving measurement speed, sensitivity and spatial resolution. In addition to optimizing existing protocols, new application areas are being explored. This includes the analysis of material from plants, insects and fungi.

References

Abrass CK (2004) Cellular lipid metabolism and the role of lipids in progressive renal disease. Am J Nephrol 24(1):46–53

Acquadro E, Cabella C, Ghiani S, Miragoli L, Bucci EM, Corpillo D (2009) Matrix-assisted laser desorption ionization imaging mass spectrometry detection of a magnetic resonance imaging contrast agent in mouse liver. Anal Chem 81(7):2779–2784. doi:10.1021/ac900038y

Aerni HR, Cornett DS, Caprioli RM (2006) Automated acoustic matrix deposition for MALDI sample preparation. Anal Chem 78(3):827–834. doi:10.1021/ac051534r

Altelaar AFM, van Minnen J, Jiménez CR, Heeren RMA, Piersma SR (2005) Direct molecular imaging of lymnaea stagnalis nervous tissue at subcellular spatial resolution by mass spectrometry. Anal Chem 77(3):735–741. doi:10.1021/ac048329g

Altelaar AFM, Klinkert I, Jalink K, de Lange RPJ, Adan RAH, Heeren RMA, Piersma SR (2006) Gold-enhanced biomolecular surface imaging of cells and tissue by SIMS and MALDI mass spectrometry. Anal Chem 78(3):734–742. doi:10.1021/ac0513111

Altelaar AFM, Taban IM, McDonnell LA, Verhaert PDEM, de Lange RPJ, Adan RAH, Mooi WJ, Heeren RMA, Piersma SR (2007) High-resolution MALDI imaging mass spectrometry allows localization of peptide distributions at cellular length scales in pituitary tissue sections. Int J Mass Spectrom 260(2–3):203–211. doi:10.1016/j.ijms.2006.09.028

Amster IJ (1996) Fourier transform mass spectrometry. J Mass Spectrom 31:1325–1337

Balluff B, Elsner M, Kowarsch A, Rauser S, Meding S, Schuhmacher C, Feith M, Herrmann K, Rocken C, Schmid RM, Hofler H, Walch A, Ebert MP (2010) Classification of HER2/neu status in gastric cancer using a breast-cancer derived proteome classifier. J Proteome Res 9(12):6317–6322

Balluff B, Rauser S, Meding S, Elsner M, Schone C, Feuchtinger A, Schuhmacher C, Novotny A, Jutting U, Maccarrone G, Sarioglu H, Ueffing M, Braselmann H, Zitzelsberger H, Schmid RM, Hofler H, Ebert MP, Walch A (2011a) MALDI imaging identifies prognostic seven-protein signature of novel tissue markers in intestinal-type gastric cancer. Am J Pathol 179(6):2720–2729. doi:10.1016/j.ajpath.2011.08.032

Balluff B, Schöne C, Höfler H, Walch A (2011b) MALDI imaging mass spectrometry for direct tissue analysis: technological advancements and recent applications. Histochem Cell Biol 136(3):227–244. doi:10.1007/s00418-011-0843-x

Benabdellah F, Touboul D, Brunelle A, Laprevote O (2009a) In situ primary metabolites localization on a rat brain section by chemical mass spectrometry imaging. Anal Chem 81(13):5557–5560. doi:10.1021/ac9005364

Benabdellah F, Yu H, Brunelle A, Laprevote O, De La Porte S (2009b) MALDI reveals membrane lipid profile reversion in MDX mice. Neurobiol Dis 36(2):252–258. doi:10.1016/j.nbd.2009.07.013

Bouschen W, Schulz O, Eikel D, Spengler B (2010) Matrix vapor deposition/recrystallization and dedicated spray preparation for high-resolution scanning microprobe matrix-assisted laser desorption/ionization imaging mass spectrometry (SMALDI-MS) of tissue and single cells. Rapid Commun Mass Spectrom 24(3):355–364

Boxer SG, Kraft ML, Weber PK (2009) Advances in imaging secondary ion mass spectrometry for biological samples. Annu Rev Biophys 38:53–74. doi:10.1146/annurev.biophys.050708.133634

Brignole-Baudouin F, Desbenoit N, Hamm G, Liang H, Both J-P, Brunelle A, Fournier I, Guerineau V, Legouffe R, Stauber J, Touboul D, Wisztorski M, Salzet M, Laprevote O, Baudouin C (2012) A new safety concern for glaucoma treatment demonstrated by mass spectrometry imaging of benzalkonium chloride distribution in the eye, an experimental study in rabbits. PLoS ONE 7(11):e50180. doi:10.1371/journal.pone.0050180

Burnum KE, Cornett DS, Puolitaival SM, Milne SB, Myers DS, Tranguch S, Brown HA, Dey SK, Caprioli RM (2009) Spatial and temporal alterations of phospholipids determined by mass spectrometry during mouse embryo implantation. J Lipid Res 50(11):2290–2298. doi:10.1194/jlr.M900100-JLR200

Burrell MM, Earnshaw CJ, Clench MR (2007) Imaging matrix assisted laser desorption ionization mass spectrometry: a technique to map plant metabolites within tissues at high spatial resolution. J Exp Bot 58(4):757–763

Caprioli RM, Farmer TB, Gile J (1997) Molecular imaging of biological samples: localization of peptides and proteins using MALDI-TOF MS. Anal Chem 69(23):4751–4760

Casadonte R, Caprioli RM (2011) Proteomic analysis of formalin-fixed paraffin-embedded tissue by MALDI imaging mass spectrometry. Nat Protoc 6(11):1695–1709

Cazares LH, Troyer D, Mendrinos S, Lance RA, Nyalwidhe JO, Beydoun HA, Clements MA, Drake RR, Semmes OJ (2009) Imaging mass spectrometry of a specific fragment of mitogen-activated protein kinase/extracellular signal-regulated kinase kinase kinase 2 discriminates cancer from uninvolved prostate tissue. Clin Cancer Res 15(17):5541–5551. doi:10.1158/1078-0432.ccr-08-2892

Chaurand P, Luetzenkirchen F, Spengler B (1999) Peptide and protein identification by matrix-assisted laser desorption ionization (MALDI) and MALDI-post-source decay time-of-flight mass spectrometry. J Am Soc Mass Spectrom 10(2):91–103

Chaurand P, Schriver KE, Caprioli RM (2007) Instrument design and characterization for high resolution MALDI-MS imaging of tissue sections. J Mass Spectrom 42(4):476–489. doi:10.1002/jms.1180

Chen RB, Hui LM, Sturm RM, Li LJ (2009) Three dimensional mapping of neuropeptides and lipids in crustacean brain by mass spectral imaging. J Am Soc Mass Spectrom 20(6):1068–1077. doi:10.1016/j.jasms.2009.01.017

Chen RB, Jiang XY, Conaway MCP, Mohtashemi I, Hui LM, Viner R, Li LJ (2010) Mass spectral analysis of neuropeptide expression and distribution in the nervous system of the lobster Homarus americanus. J Proteome Res 9(2):818–832. doi:10.1021/pr900736t

Chughtai K, Heeren RMA (2010) Mass spectrometric imaging for biomedical tissue analysis. Chem Rev 110(5):3237–3277

Colliver TL, Brummel CL, Pacholski ML, Swanek FD, Ewing AG, Winograd N (1997) Atomic and molecular imaging at the single-cell level with TOF-SIMS. Anal Chem 69(13):2225–2231. doi:10.1021/ac9701748

Cornett DS, Frappier SL, Caprioli RM (2008) MALDI-FTICR imaging mass spectrometry of drugs and metabolites in tissue. Anal Chem 80(14):5648–5653. doi:10.1021/ac800617s

Debois D, Bertrand V, Quinton L, De Pauw-Gillet MC, De Pauw E (2010) MALDI-in source decay applied to mass spectrometry imaging: a new tool for protein identification. Anal Chem 82(10):4036–4045. doi:10.1021/ac902875q

DeKeyser SS, Kutz-Naber KK, Schmidt JJ, Barrett-Wilt GA, Li LJ (2007) Imaging mass spectrometry of neuropeptides in decapod crustacean neuronal tissues. J Proteome Res 6(5):1782–1791. doi:10.1021/pr060603v

Djidja MC, Francese S, Loadman PM, Sutton CW, Scriven P, Claude E, Snel MF, Franck J, Salzet M, Clench MR (2009) Detergent addition to tryptic digests and ion mobility separation prior to MS/MS improves peptide yield and protein identification for in situ proteomic investigation of frozen and formalin-fixed paraffin-embedded adenocarcinoma tissue sections. Proteomics 9(10):2750–2763. doi:10.1002/pmic.200800624

Djidja M-C, Claude E, Snel MF, Francese S, Scriven P, Carolan V, Clench MR (2010) Novel molecular tumour classification using MALDI-mass spectrometry imaging of tissue micro-array. Anal Bioanal Chem 397(2):587–601. doi:10.1007/s00216-010-3554-6

Eberlin LS, Ifa DR, Wu C, Cooks RG (2010) Three-dimensional visualization of mouse brain by lipid analysis using ambient ionization mass spectrometry. Angew Chem Int Ed 49(5):873–876. doi:10.1002/anie.200906283

El Ayed M, Bonnel D, Longuespee R, Castellier C, Franck J, Vergara D, Desmons A, Tasiemski A, Kenani A, Vinatier D, Day R, Fournier I, Salzet M (2010) MALDI imaging mass spectrometry in ovarian cancer for tracking, identifying, and validating biomarkers. Med Sci Monit 16(8):BR233–BR245

Esquenazi E, Coates C, Simmons L, Gonzalez D, Gerwick WH, Dorrestein PC (2008) Visualizing the spatial distribution of secondary metabolites produced by marine cyanobacteria and sponges via MALDI-TOF imaging. Mol BioSyst 4(6):562–570

Fenn J, Mann M, Meng C, Wong S, Whitehouse C (1989) Electrospray ionization for mass spectrometry of large biomolecules. Science 246(4926):64–71. doi:10.1126/science.2675315

Francese S, Dani FR, Traldi P, Mastrobuoni G, Pieraccini G, Moneti G (2009) MALDI mass spectrometry imaging, from its origins up to today: the state of the art. Comb Chem High Throughput Screen 12(2):156–174

Franck J, El Ayed M, Wisztorski M, Salzet M, Fournier I (2009) On-tissue N-terminal peptide derivatization for enhancing protein identification in MALDI mass spectrometric imaging strategies. Anal Chem 81(20):8305–8317. doi:10.1021/ac901043n

Franck J, Longuespee R, Wisztorski M, Van Remoortere A, Van Zeijl R, Deelder A, Salzet M, McDonnell L, Fournier I (2010) MALDI mass spectrometry imaging of proteins exceeding 30 000 daltons. Med Sci Monit 16(9):BR293–BR299

Froesch M, Luxembourg SL, Verheijde D, Heeren RM (2010) Imaging mass spectrometry using a delay-line detector. Eur J Mass Spectrom 16(1):35–45

Grey AC, Chaurand P, Caprioli RM, Schey KL (2009) MALDI imaging mass spectrometry of integral membrane proteins from ocular lens and retinal tissue. J Proteome Res 8(7):3278–3283. doi:10.1021/pr800956y

Groseclose MR, Andersson M, Hardesty WM, Caprioli RM (2007) Identification of proteins directly from tissue: in situ tryptic digestions coupled with imaging mass spectrometry. J Mass Spectrom 42(2):254–262. doi:10.1002/jms.1177

Guenther S, Koestler M, Schulz O, Spengler B (2010) Laser spot size and laser power dependence of ion formation in high resolution MALDI imaging. Int J Mass Spectrom 294(1):7–15. doi:10.1016/j.ijms.2010.03.014

Guenther S, Römpp A, Kummer W, Spengler B (2011) AP-MALDI imaging of neuropeptides in mouse pituitary gland with 5 um spatial resolution and high mass accuracy. Int J Mass Spectrom 305(2–3):228–237. doi:10.1016/j.ijms.2010.11.011

Gustafsson JOR, Oehler MK, McColl SR, Hoffmann P (2010) Citric acid antigen retrieval (CAAR) for tryptic peptide imaging directly on archived formalin-fixed paraffin-embedded tissue. J Proteome Res 9(9):4315–4328. doi:10.1021/Pr9011766

He F, Hendrickson CL, Marshall AG (2001) Baseline mass of peptide isobars: a record for molecular mass resolution. Anal Chem 73(3):647–650

Hillenkamp F, Unsold E, Kaufmann R, Nitsche R (1975a) High-sensitivity laser microprobe mass analyzer. Appl Phys 8(4):341–348. doi:10.1007/bf00898368

Hillenkamp F, Unsold E, Kaufmann R, Nitsche R (1975b) Laser microprobe mass analysis of organic materials. Nature 256(5513):119–120. doi:10.1038/256119a0

Hochheiser H, Yanowitz J (2007) If I only had a brain: exploring mouse brain images in the Allen Brain Atlas. Biol Cell 99(7):403–409. doi:10.1042/bc20070031

Imabiotech (2012) Quantinetix MALDI imaging software. http://www.imabiotech.com/Quantinetix-TM-Maldi-Imaging.html?lang=en. Accessed 8 July 2012

Invitrogen (2011) Invitrogen product information DiOC6(3) http://products.invitrogen.com/ivgn/product/D273. Accessed 15 Dec 2011

Jackson SN, Wang HYJ, Woods AS (2005) In situ structural characterization of phosphatidylcholines in brain tissue using MALDI-MS/MS. J Am Soc Mass Spectrom 16(12):2052–2056. doi:10.1016/j.jasms.2005.08.014

Jurchen JC, Rubakhin SS, Sweedler JV (2005) MALDI-MS imaging of features smaller than the size of the laser beam. J Am Soc Mass Spectrom 16(10):1654–1659. doi:10.1016/j.jasms.2005.06.006

Karas M, Hillenkamp F (1988) Laser desorption ionization of proteins with molecular masses exceeding 10000 daltons. Anal Chem 60(20):2299–2301. doi:10.1021/ac00171a028

Karas M, Bachmann D, Hillenkamp F (1985) Influence of the wavelength in high-irradiance ultraviolet laser desorption mass spectrometry of organic molecules. Anal Chem 57(14):2935–2939. doi:10.1021/ac00291a042

Kaspar S, Peukert M, Svatos A, Matros A, Mock H-P (2011) MALDI-imaging mass spectrometry—an emerging technique in plant biology. Proteomics 11(9):1840–1850. doi:10.1002/pmic.201000756

Kawamoto T (2003) Use of a new adhesive film for the preparation of multi-purpose fresh-frozen sections from hard tissues, whole-animals, insects and plants. Arch Histol Cytol 66(2):123–143

Khatib-Shahidi S, Andersson M, Herman JL, Gillespie TA, Caprioli RM (2006) Direct molecular analysis of whole-body animal tissue sections by imaging MALDI mass spectrometry. Anal Chem 78(18):6448–6456. doi:10.1021/ac060788p

Koestler M, Kirsch D, Hester A, Leisner A, Guenther S, Spengler B (2008) A high-resolution scanning microprobe matrix-assisted laser desorption/ionization ion source for imaging analysis on an ion trap/Fourier transform ion cyclotron resonance mass spectrometer. Rapid Commun Mass Spectrom 22(20):3275–3285. doi:10.1002/rcm.3733

Laiko VV, Baldwin MA, Burlingame AL (2000) Atmospheric pressure matrix-assisted laser desorption/ionization mass spectrometry. Anal Chem 72(4):652–657. doi:10.1021/ac990998k

Landgraf RR, Conaway MCP, Garrett TJ, Stacpoole PW, Yost RA (2009) Imaging of lipids in spinal cord using intermediate pressure matrix-assisted laser desorption-linear ion trap/Orbitrap MS. Anal Chem 81(20):8488–8495. doi:10.1021/ac901387u

Lee C-H, Olson P, Evans RM (2003) Minireview: lipid metabolism, metabolic diseases, and peroxisome proliferator-activated receptors. Endocrinology 144(6):2201–2207. doi:10.1210/en.2003-0288

Lee YJ, Perdian DC, Song Z, Yeung ES, Nikolau BJ (2012) Use of mass spectrometry for imaging metabolites in plants. Plant J 70(1):81–95. doi:10.1111/j.1365-313X.2012.04899.x

Leinweber BD, Tsaprailis G, Monks TJ, Lau SS (2009) Improved MALDI-TOF imaging yields increased protein signals at high molecular mass. J Am Soc Mass Spectrom 20(1):89–95. doi:10.1016/j.jasms.2008.09.008

Lemaire R, Wisztorski M, Desmons A, Tabet JC, Day R, Salzet M, Fournier I (2006) MALDI-MS direct tissue analysis of proteins: improving signal sensitivity using organic treatments. Anal Chem 78(20):7145–7153

Lemaire R, Desmons A, Tabet JC, Day R, Salzet M, Fournier I (2007a) Direct analysis and MALDI imaging of formalin-fixed, paraffin-embedded tissue sections. J Proteome Res 6(4):1295–1305. doi:10.1021/pr060549i

Lemaire R, Menguellet SA, Stauber J, Marchaudon V, Lucot JP, Collinet P, Farine MO, Vinatier D, Day R, Ducoroy P, Salzet M, Fournier I (2007b) Specific MALDI imaging and profiling for biomarker hunting and validation: fragment of the 11S proteasome activator complex, reg alpha fragment, is a new potential ovary cancer biomarker. J Proteome Res 6(11):4127–4134. doi:10.1021/pr0702722

Liu Y, Ma X, Lin Z, He M, Han G, Yang C, Xing Z, Zhang S, Zhang X (2010) Imaging mass spectrometry with a low-temperature plasma probe for the analysis of works of art. Angew Chem Int Ed 49(26):4435–4437. doi:10.1002/anie.200906975

Loboda AV, Krutchinsky AN, Bromirski M, Ens W, Standing KG (2000) A tandem quadrupole/time-of-flight mass spectrometer with a matrix-assisted laser desorption/ionization source: design and performance. Rapid Commun Mass Spectrom 14(12):1047–1057

Luxembourg SL, Mize TH, McDonnell LA, Heeren RMA (2004) High-spatial resolution mass spectrometric imaging of peptide and protein distributions on a surface. Anal Chem 76(18):5339–5344. doi:10.1021/ac049692q

Makarov A (2000) Electrostatic axially harmonic orbital trapping: a high-performance technique of mass analysis. Anal Chem 72(6):1156–1162. doi:10.1021/ac991131p

Makarov A, Denisov E, Lange O, Horning S (2006) Dynamic range of mass accuracy in LTQ Orbitrap hybrid mass spectrometer. J Am Soc Mass Spectrom 17(7):977–982. doi:10.1016/j.jasms.2006.03.006

Mange A, Chaurand P, Perrochia H, Roger P, Caprioli RM, Solassol J (2009) Liquid chromatography-tandem and MALDI imaging mass spectrometry analyses of RCL2/CS100-fixed, paraffin-embedded tissues: proteomics evaluation of an alternate fixative for biomarker discovery. J Proteome Res 8(12):5619–5628. doi:10.1021/pr9007128

Marshall AG (2000) Milestones in Fourier transform ion cyclotron resonance mass spectrometry technique development. Int J Mass Spectrom 200(1–3):331–356

Marshall AG, Hendrickson CL (2002) Fourier transform ion cyclotron resonance detection: principles and experimental configurations. Int J Mass Spectrom 215(1–3):59–75

Martens L, Chambers M, Sturm M, Kessner D, Levander F, Shofstahl J, Tang WH, Rompp A, Neumann S, Pizarro AD, Montecchi-Palazzi L, Tasman N, Coleman M, Reisinger F, Souda P, Hermjakob H, Binz P-A, Deutsch EW (2011) mzML—a community standard for mass spectrometry data. Mol Cell Proteomics 10(1). doi:10.1074/mcp.R1110.000133

McDonnell LA, Heeren RMA (2007) Imaging mass spectrometry. Mass Spectrom Rev 26(4):606–643. doi:10.1002/mas.20124

McDonnell LA, Corthals GL, Willems SM, van Remoortere A, van Zeijl RJM, Deelder AM (2010) Peptide and protein imaging mass spectrometry in cancer research. J Proteomics 73(10):1921–1944. doi:10.1016/j.jprot.2010.05.007

Miura D, Fujimura Y, Yamato M, Hyodo F, Utsumi H, Tachibana H, Wariishi H (2010) Ultrahighly sensitive in situ metabolomic imaging for visualizing spatiotemporal metabolic behaviors. Anal Chem 82(23):9789–9796. doi:10.1021/ac101998z

Monroe EB, Annangudi SR, Hatcher NG, Gutstein HB, Rubakhin SS, Sweedler JV (2008) SIMS and MALDI MS imaging of the spinal cord. Proteomics 8(18):3746–3754. doi:10.1002/pmic.200800127

Ostrowski SG, Van Bell CT, Winograd N, Ewing AG (2004) Mass spectrometric imaging of highly curved membranes during Tetrahymena mating. Science 305(5680):71–73. doi:10.1126/science.1099791

Paradisi G, Ianniello F, Tomei C, Bracaglia M, Carducci B, Gualano MR, La Torre G, Banci M, Caruso A (2010) Longitudinal changes of adiponectin, carbohydrate and lipid metabolism in pregnant women at high risk for gestational diabetes. Gynecol Endocrinol 26(7):539–545. doi:10.3109/09513591003632084

Paschke C, Leisner A, Hester A, Maass K, Guenther S, Bouschen W, Spengler B (submitted) A software package for automatic processing of mass spectrometric images. J Am Soc Mass Spectrom

Peukert M, Matros A, Lattanzio G, Kaspar S, Abadía J, Mock H-P (2011) Spatially resolved analysis of small molecules by matrix-assisted laser desorption/ionization mass spectrometric imaging (MALDI-MSI). New Phytol 193(3):806–815. doi:10.1111/j.1469-8137.2011.03970.x

Pól J, Strohalm M, Havlíček V, Volný M (2010) Molecular mass spectrometry imaging in biomedical and life science research. Histochem Cell Biol 134(5):423–443. doi:10.1007/s00418-010-0753-3

PREMIERBiosoft (2012) MALDIVision. http://www.premierbiosoft.com/maldi-tissue-imaging/index.html. Accessed 3 July 2012

Prideaux B, Stoeckli M (2012) Mass spectrometry imaging for drug distribution studies. J Proteomics 75(16):4999–5013. doi:10.1016/j.jprot.2012.07.028

Prideaux B, Dartois V, Staab D, Weiner DM, Goh A, Via LE, Barry CE III, Stoeckli M (2011) High-sensitivity MALDI-MRM-MS imaging of moxifloxacin distribution in tuberculosis-infected rabbit lungs and granulomatous lesions. Anal Chem 83(6):2112–2118. doi:10.1021/ac1029049

Rauser S, Deininger S-O, Suckau D, Hoefler H, Walch A (2010a) Approaching MALDI molecular imaging for clinical proteomic research: current state and fields of application. Expert Rev Proteomics 7(6):927–941. doi:10.1586/epr.10.83

Rauser S, Marquardt C, Balluff B, Deininger SO, Albers C, Belau E, Hartmer R, Suckau D, Specht K, Ebert MP, Schmitt M, Aubele M, Hofler H, Walch A (2010b) Classification of HER2 receptor status in breast cancer tissues by MALDI imaging mass spectrometry. J Proteome Res 9(4):1854–1863

Reyzer ML, Caprioli RM (2007) MALDI-MS-based imaging of small molecules and proteins in tissues. Curr Opin Chem Biol 11(1):29–35. doi:10.1016/j.cbpa.2006.11.035

Richards AL, Lietz CB, Wager-Miller JB, Mackie K, Trimpin S (2011) Imaging mass spectrometry in transmission geometry. Rapid Commun Mass Spectrom 25(6):815–820. doi:10.1002/rcm.4927

Riedelsheimer B, Wegerhoff R, van den Boom F, Welsch U (2010) Romeis—Mikroskopische Technik, 18th edn. Spektrum Akademischer Verlag, Heidelberg

Rohner TC, Staab D, Stoeckli M (2005) MALDI mass spectrometric imaging of biological tissue sections. Mech Ageing Dev 126(1):177–185. doi:10.1016/j.mad.2004.09.032

Römpp A, Taban IM, Mihalca R, Duursma MC, Mize TH, McDonnell LA, Heeren RMA (2005) Examples of Fourier transform ion cyclotron resonance mass spectrometry developments: from ion physics to remote access biochemical mass spectrometry. Eur J Mass Spectrom 11(5):443–456. doi:10.1255/ejms.732

Römpp A, Dekker L, Taban I, Jenster G, Boogerd W, Bonfrer H, Spengler B, Heeren R, Smitt PS, Luider TM (2007) Identification of leptomeningeal metastasis-related proteins in cerebrospinal fluid of patients with breast cancer by a combination of MALDI-TOF, MALDI-FTICR and nanoLC-FTICR MS. Proteomics 7(3):474–481. doi:10.1002/pmic.200600719

Römpp A, Guenther S, Schober Y, Schulz O, Takats Z, Kummer W, Spengler B (2010a) Histology by mass spectrometry: label-free tissue characterization obtained from high-accuracy bioanalytical imaging. Angew Chem Int Ed 49(22):3834–3838

Römpp A, Schramm T, Hester A, Klinkert I, Heeren R, Stöckli M, Both J-P, Brunelle A, Spengler B (2010b) Imaging mzML (imzML)—a common data format for imaging mass spectrometry. In: Hamacher M, Stephan C, Eisenacher M (eds) Data mining in proteomics. Methods in molecular biology. Humana Press, New York, pp 205–224

Römpp A, Guenther S, Schober Y, Takats Z, Kummer W, Spengler B (2010b) Fourier transform mass spectrometry of biological samples at cellular resolution. In: Proceedings of 58th ASMS conference on mass spectrometry. Salt Lake City, Utah, USA, May 23–27

Römpp A, Guenther S, Schober Y, Kokesch J, Bhandari D, Takats Z, Spengler B (2011a) Mass spectrometry imaging with high resolution in mass and space (HR^2 MSI)—a new level of information and validity. In: Proceedings of the 59th ASMS conference on mass spectrometry and allied topics. Denver, CO, USA, June 5–9

Römpp A, Guenther S, Takats Z, Spengler B (2011b) Mass spectrometry imaging with high resolution in mass and space (HR^2 MSI) for reliable investigation of drug compound distributions on the cellular level. Anal Bioanal Chem. doi:10.1007/s00216-011-4990-7

Santos CR, Schulze A (2012) Lipid metabolism in cancer. FEBS J 279(15):2610–2623. doi:10.1111/j.1742-4658.2012.08644.x

Schober Y, Schramm T, Spengler B, Roempp A (2011) Protein identification by accurate mass matrix-assisted laser desorption/ionization imaging of tryptic peptides. Rapid Commun Mass Spectrom 25(17):2475–2483. doi:10.1002/rcm.5135

Schober Y, Guenther S, Spengler B, Römpp A (2012a) High-resolution matrix-assisted laser desorption/ionization imaging of tryptic peptides from tissue. Rapid Commun Mass Spectrom 26(9):1141–1146. doi:10.1002/rcm.6192

Schober Y, Guenther S, Spengler B, Römpp A (2012b) Single cell matrix-assisted laser desorption/ionization mass spectrometry imaging. Anal Chem 84(15):6293–6297. doi:10.1021/ac301337h

Schramm T, Hester A, Klinkert I, Both J-P, Heeren RMA, Brunelle A, Laprévote O, Desbenoit N, Robbe M-F, Stoeckli M, Spengler B, Römpp A (2012) imzML—a common data format for the flexible exchange and processing of mass spectrometry imaging

data. J Proteomics 75(16):5106–5110. doi:10.1016/j.jprot.2012.07.026

Schuerenberg M, Luebbert C, Deininger S-O, Ketterlinus R, Suckau D (2007) MALDI tissue imaging: mass spectrometric localization of biomarkers in tissue slices. Nat Meth 4(5):3–4

Schwamborn K (2012) Imaging mass spectrometry in biomarker discovery and validation. J Proteomics 75(16):4990–4998. doi:10.1016/j.jprot.2012.06.015

Schwartz SA, Reyzer ML, Caprioli RM (2003) Direct tissue analysis using matrix-assisted laser desorption/ionization mass spectrometry: practical aspects of sample preparation. J Mass Spectrom 38(7):699–708. doi:10.1002/jms.505

Shimma S, Sugiura Y, Hayasaka T, Zaima N, Matsumoto M, Setou M (2008) Mass imaging and identification of biomolecules with MALDI-QIT-TOF-based system. Anal Chem 80(3):878–885

Shroff R, Vergara F, Muck A, SvatoǍ A, Gershenzon J (2008) Nonuniform distribution of glucosinolates in Arabidopsis thaliana leaves has important consequences for plant defense. Proc Natl Acad Sci USA 105(16):6196–6201. doi:10.1073/pnas.0711730105

Sidman RL (2011) High resolution mouse brain atlas. http://www.hms.harvard.edu/research/brain/people.html

Smith B, Ashburner M, Rosse C, Bard J, Bug W, Ceusters W, Goldberg LJ, Eilbeck K, Ireland A, Mungall CJ, Leontis N, Rocca-Serra P, Ruttenberg A, Sansone SA, Scheuermann RH, Shah N, Whetzel PL, Lewis S, Consortium OBI (2007) The OBO foundry: coordinated evolution of ontologies to support biomedical data integration. Nat Biotechnol 25(11):1251–1255. doi:10.1038/nbt1346

Snel MF, Fuller M (2010) High-spatial resolution matrix-assisted laser desorption ionization imaging analysis of glucosylceramide in spleen sections from a mouse model of Gaucher disease. Anal Chem 82(9):3664–3670. doi:10.1021/ac902939k

Solon EG, Schweitzer A, Stoeckli M, Prideaux B (2010) Autoradiography, MALDI-MS, and SIMS-MS imaging in pharmaceutical discovery and development. AAPS J 12(1):11–26. doi:10.1208/s12248-009-9158-4

Sparvero LJ, Amoscato AA, Kochanek PM, Pitt BR, Kagan VE, Bayır H (2010) Mass-spectrometry based oxidative lipidomics and lipid imaging: applications in traumatic brain injury. J Neurochem 115(6):1322–1336. doi:10.1111/j.1471-4159.2010.07055.x

Spengler B, Hubert M (2002) Scanning microprobe matrix-assisted laser desorption ionization (SMALDI) mass spectrometry: instrumentation for sub-micrometer resolved LDI and MALDI surface analysis. J Am Soc Mass Spectrom 13(6):735–748

Spengler B, Hubert M, Kaufmann R (1994) MALDI ion imaging and biological ion imaging with a new scanning UV-laser microprobe. In: Proceedings of the 42nd annual conference on mass spectrometry and allied topics. Chicago, Illinois, May 29–June 3

Stauber J, Lemaire R, Franck J, Bonnel D, Croix D, Day R, Wisztorski M, Fournier I, Salzet M (2008) MALDI imaging of formalin-fixed paraffin-embedded tissues: application to model animals of Parkinson disease for biomarker hunting. J Proteome Res 7(3):969–978. doi:10.1021/pr070464x

Stauber J, MacAleese L, Franck J, Claude E, Snel M, Kaletas BK, Wiel IMVD, Wisztorski M, Fournier I, Heeren RMA (2010) On-tissue protein identification and imaging by MALDI-ion mobility mass spectrometry. J Am Soc Mass Spectrom 21(3):338–347

Stoeckli M, Chaurand P, Hallahan DE, Caprioli RM (2001) Imaging mass spectrometry: a new technology for the analysis of protein expression in mammalian tissues. Nat Med 7(4):493–496

Stoeckli M, Staab D, Staufenbiel M, Wiederhold K-H, Signor L (2002) Molecular imaging of amyloid [beta] peptides in mouse brain sections using mass spectrometry. Anal Biochem 311(1):33–39. doi:10.1016/s0003-2697(02)00386-x

Stoeckli M, Staab D, Schweitzer A (2007a) Compound and metabolite distribution measured by MALDI mass spectrometric imaging in whole-body tissue sections. Int J Mass Spectrom 260(2–3):195–202. doi:10.1016/j.ijms.2006.10.007

Stoeckli M, Staab D, Schweitzer A, Gardiner J, Seebach D (2007b) Imaging of a beta-peptide distribution in whole-body mice sections by MALDI mass spectrometry. J Am Soc Mass Spectrom 18(11):1921–1924. doi:10.1016/j.jasms.2007.08.005

Strohalm M, Strohalm J, Kaftan F, Krasny L, Volny M, Novak P, Ulbrich K, Havlicek V (2011) Poly N-(2-hydroxypropyl)methacrylamide -based tissue-embedding medium compatible with MALDI mass spectrometry imaging experiments. Anal Chem 83(13):5458–5462. doi:10.1021/ac2011679

Szakal C, Narayan K, Fu J, Lefman J, Subramaniam S (2011) Compositional mapping of the surface and interior of mammalian cells at submicrometer resolution. Anal Chem 83(4):1207–1213. doi:10.1021/ac1030607

Taban IM, Altelaar AFM, Van der Burgt YEM, McDonnell LA, Heeren RMA, Fuchser J, Baykut G (2007) Imaging of peptides in the rat brain using MALDI-FTICR mass spectrometry. J Am Soc Mass Spectrom 18(1):145–151. doi:10.1016/j.jasms.2006.09.017

Thomas A, Charbonneau JL, Fournaise E, Chaurand P (2012) Sublimation of new matrix candidates for high spatial resolution imaging mass spectrometry of lipids: enhanced information in both positive and negative polarities after 1,5-diaminonapthalene deposition. Anal Chem 84(4):2048–2054. doi:10.1021/ac2033547

Trim PJ, Atkinson SJ, Princivalle AP, Marshall PS, West A, Clench MR (2008) Matrix-assisted laser desorption/ionisation mass spectrometry imaging of lipids in rat brain tissue with integrated unsupervised and supervised multivariant statistical analysis. Rapid Commun Mass Spectrom 22(10):1503–1509. doi:10.1002/rcm.3498

Trim PJ, Djidja MC, Atkinson SJ, Oakes K, Cole LM, Anderson DMG, Hart PJ, Francese S, Clench MR (2010) Introduction of a 20 kHz Nd:YVO4 laser into a hybrid quadrupole time-of-flight mass spectrometer for MALDI-MS imaging. Anal Bioanal Chem 397(8):3409–3419. doi:10.1007/s00216-010-3874-6

van Remoortere A, van Zeijl RJM, van den Oever N, Franck J, Longuespee R, Wisztorski M, Salzet M, Deelder AM, Fournier I, McDonnell LA (2010) MALDI imaging and profiling MS of higher mass proteins from tissue. J Am Soc Mass Spectrom 21(11):1922–1929. doi:10.1016/j.jasms.2010.07.011

Vanickova L, Svatos A, Kroiss J, Kaltenpoth M, Do Nascimento RR, Hoskovec M, Brizova R, Kalinova B (2012) Cuticular hydrocarbons of the South American fruit fly Anastrepha fraterculus: variability with sex and age. J Chem Ecol 38(9):1133–1142. doi:10.1007/s10886-012-0177-8

Vazquez-Boland JA, Kuhn M, Berche P, Chakraborty T, Dominguez-Bernal G, Goebel W, Gonzalez-Zorn B, Wehland J, Kreft J (2001) Listeria pathogenesis and molecular virulence determinants. Clin Microbiol Rev 14(3):584. doi:10.1128/cmr.14.3.584-640.2001

Verhaert PD, Conaway MCP, Pekar TM, Miller K (2007) Neuropeptide imaging on an LTQ with vMALDI source: the complete 'all-in-one' peptidome analysis. Int J Mass Spectrom 260(2–3):177–184. doi:10.1016/j.ijms.2006.11.008

Walch A, Rauser S, Deininger S-O, Hoefler H (2008) MALDI imaging mass spectrometry for direct tissue analysis: a new frontier for molecular histology. Histochem Cell Biol 130(3):421–434. doi:10.1007/s00418-008-0469-9

Watrous JD, Alexandrov T, Dorrestein PC (2011) The evolving field of imaging mass spectrometry and its impact on future biological research. J Mass Spectrom 46(2):209–222. doi:10.1002/jms.1876

Yang J, Caprioli RM (2011) Matrix sublimation/recrystallization for imaging proteins by mass spectrometry at high spatial resolution. Anal Chem 83(14):5728–5734. doi:10.1021/ac200998a

Yang Y-L, Xu Y, Straight P, Dorrestein PC (2009) Translating metabolic exchange with imaging mass spectrometry. Nat Chem Biol 5(12):885–887

Zimmerman TA, Rubakhin SS, Sweedler JV (2011) MALDI mass spectrometry imaging of neuronal cell cultures. J Am Soc Mass Spectrom 22(5):828–836. doi:10.1007/s13361-011-0111-2

Zubarev R, Mann M (2007) On the proper use of mass accuracy in proteomics. Mol Cell Proteomics 6(3):377–381